Electronic Supplementary Material (ESI) for Dalton Transactions.

Supporting Information

Synthesis of M-UiO-66 (M = Zr, Ce or Hf) employing 2,5-pyridinedicarboxylic acid as linker: defect chemistry, framework hydrophilisation and sorption properties

S. Waitschat[a]*, D. Fröhlich*[b]*, H. Reinsch*[a]*,* H. Terraschke[a], K. A. Lomachenko[c,d], C. Lamberti[d,e], *H. Kummer*[b]*, T. Helling*[b]*, M. Baumgartner*[b]*, S. Henninger*[b] *and N. Stock*[a*]

[a] *Institut für Anorganische Chemie, Christian-Albrechts-Universität,*
Max-Eyth-Straße 2, D 24118 Kiel, Germany
[b] *Fraunhofer-Institute for Solar Energy Systems ISE, Heidenhofstrasse 2, 79110 Freiburg, Germany*
[c] *European Synchrotron Radiation Facility, 71 Avenue des Martyrs, CS 40220, 38043 Grenoble Cedex 9, France*
[d] *IRC "Smart Materials", Southern Federal University, Zorge str. 5, 344090 Rostov-on-Don, Russia*
[e] *Department of Chemistry, CrisDi Centre and INSTM Reference Center, University of Turin, Via Giuria 7, 10125 Turin, Italy*

Prof. Dr. Norbert Stock, Tel.: +49-431-880-1675, Fax: +49-431-880-1775,
Email: stock@ac.uni-kiel.de

Table of Contents

S1 Methods and Reagents

Initial characterization was performed using a Stoe Stadi P X-ray diffractometer equipped with a xy-stage in transmission geometry using Mo $K_{\alpha1}$ radiation and with data collected by a Mythen detector. Powder X-Ray Diffraction (PXRD) patterns for structure determination were measured using a Stoe Stadi P diffractometer in transmission geometry using Cu $K_{\alpha1}$ radiation and with data collected using a Mythen detector. Infrared spectra were recorded on a Bruker ALPHA-P A220/D-01 FTIR spectrometer fitted with an ATR unit, over the spectral range of 4000-400 cm^{-1}. Thermogravimetric analysis was carried out using a NETZSCH STA 429 CD analyzer with a heating rate of 4 K min^{-1} and under flowing air (flow rate 75 ml min^{-1}). Elemental analysis was performed using a EuroVector EuroEA elemental analyzer. NMR spectroscopy was performed using a Bruker DRX 500 spectrometer. Scanning Electron Micrographs were recorded using an SEM, Zeiss Ultra Plus with FE-gun. Sorption isotherms were measured at -196 °C for N_2 and 25 °C for CO_2 with a BELSORP-max apparatus (BEL Japan Inc.). MeOH sorption isotherm were obtained with a Quantachrome Autosorb and H_2O sorption isotherms with a Quantachrome Hydrosorb at 25 °C. Powder cycle stabilities were examined in a Setaram™ TGA-DSC-111. A humidified argon gas flow (40 °C, 76.3% relative humidity) was generated by a Setaram™ WetSys humidity controller and passed through the sample chamber, while the temperature of the sample chamber itself was varied. For multi-cycle ad/desorption experiments, the temperature of the sample chamber was varied between 40 °C and 140 °C with a cycle time of 5 h. Methanol cycle stability was examined in a Surface Measurement Systems Ltd. DVS Vacuum. Before and after cycling, the sample was degassed at 90 °C in vacuum and equilibrium points were taken at 25 °C by increasing the pressure of the gas flow of 5 ml/min was held constant at 115 hPa while varying the temperature of the sample between 25 °C and 100 °C, which correspondents to a relative pressure p/p0 of 0.671 and 0.033, with cycle times of 1 h while cooling an 1 h when heating. Luminescence measurments of the solid samples have been carried out in Suprasil A quartz ampoules, at room temperature. For this purpose, a FL-22 Fluorolog3 spectrometer (HORIBA Jobin Yvon GmbH), equipped with a 450 W yenon lamp, a R928P Photomultiplier and an iHR-320-FA triple grating imaging spectrograph was applied. Reflection spectra were also recorded at room temperature from the powdered sample with a Cary 5000 spectrometer (Varian Techtron Pty.) applying BaSo4 as reference and diluting material.

Ce L_3-edge XANES measurements of Ce-UiO-66-PDC and Ce(IV) oxide were performed in the Southern Federal University (Rostov-on-Don, Russia) using Rigaku R-XAS spectrometer. X-ray tube with fixed water-cooled tungsten anode was operating at 12 kV and 80 mA. Incident X-ray beam was monochromatized by a single Johansson-type Ge (220) crystal, ensuring energy resolution of around 1 eV at 5730 eV. Measurements were conducted in transmission mode using an Ar-filled ionization chamber and a scintillation counter to monitor the intensity of incident (I_0) and transmitted (I_1) radiation respectively. Helium-filled bag filled the space between the X-ray tube, the monochromator and I_0 detector to reduce the X-rays absorption in air.

Ce(III) nitrate XANES spectrum was collected at the BM23 beamline [4] of the European Synchrotron Radiation Facility (Grenoble, France) in transmission mode using Si (111) double-crystal monochromator, Si mirrors for harmonics rejection and N_2/He-filled ionization chambers for photon detection, yielding comparable resolution with laboratory measurements.

Experimental Zr K-edge (17998 eV) EXAFS spectrum of cubic Zr-UiO-66-PDC was collected at BM23 beamline [4] of the ESRF. The ring was operating in 16-bunch regime with 90 mA maximum current. Experiment was conducted in transmission mode using Ar/He-filled ionization chambers as detectors. Gas pressure in the chambers was 0.4 bar Ar and 1.6 bar He for I_0 and 2 bar of Ar for I_1 resulting in roughly 20% and 70% absorption respectively. Si (111) double-crystal monochromator was used for energy scanning, while Rh-coated mirrors positioned at 3 mrad incidence angle were employed for harmonic rejection. The sample was prepared in the form of self-supporting pellet (13 mm diameter, 80 mg of powder, pressure < 500 kg) resulting in the edge jump of 1.5. Measurements were conducted at room temperature. Sampling step was set to 5 eV for the pre-edge and 0.5 eV in the edge region. In the EXAFS region the spectra were collected with a constant k step of $\Delta k = 0.035$ Å^{-1}. Integration time was set to 1 s/point in all spectral region. A total of 6 spectra were collected and averaged before the normalization. Excellent performance of the beamline allowed the data collection up to k=23 Å^{-1} with high signal-to-noise ratio.

Table S1.1. List of reagents used in the synthesis and their suppliers.

Reagent	Supplier	Reagent	Supplier
$Zr(SO_4)_2 \cdot 4H_2O$	ABCR	Formic acid	BASF
$ZrOCl_2 \cdot 8H_2O$	ABCR	Acetic acid	VWR
$ZrCl_4$	ABCR	HCl	Walter CMP
$ZrO(NO_3)_2 \cdot xH_2O$	ABCR	Benzoic acid	Merck
$Zr(OH)_2CO_3 \cdot ZrO_2$	Riedel-de Haen AG	NaOH	Grüssing
$(NH_4)_2[Ce(NO_3)_6]$	Alfa Aesar	Ethanol	Walter CMP
$HfCl_4$	ABCR	Dimethylformamide	Grüssing
Dichloromethane	Walter CMP	Acetonitrile	Sigma-Aldrich
Tetrahydrofuran	Walter CMP	Acetone	Walter CMP
n-Hexane	Walter CMP	Dimethylsulfoxide	Grüssing
Toluol	Walter CMP	Ethyl-acetate	Walter CMP

S2 Discovery, Optimization and Synthesis of Zr-UiO-66-PDC

The systematic investigation of the chemical system Zr^{4+}/H_2PDC (H_2L)/H_2O/modulator was carried out in a Teflon-lined high-throughput autoclave. DMF as solvent or DMF/water mixtures did not yield Zr-UiO-66-PDC, hence other investigations were carried out in water as the solvent. To optimize the reaction conditions, different metal salts as zirconium source were tested ($Zr(SO_4)_2\cdot4H_2O$, $ZrO(NO_3)_2\cdot xH_2O$, $ZrCl_4$, $ZrOCl_2\cdot8H_2O$ and $Zr(CO_3)_2$). Additionally different metal to linker ratios (1:1, 1:2, 1:3) and different modulator (FA = formic acid) to water ratios were investigated (Tab. S2.1. to Tab. S2.5.). With all metal sources Zr-UiO-66-PDC could be obtained, albeit with different crystallinity, using similar formic acid to water ratios (≈ 90 % FA) and metal to linker ratios (1:2). For all syntheses, the reaction time was set to 24 h and the reaction temperature to 120 °C. Figure S2.1. shows the PXRD pattern of Zr-UiO-66-PDC products obtained employing the optimized reaction conditions with different Zr-salts. Since the synthesis of Zr-UiO-66-PDC with $ZrOCl_2$ showed the product of highest crystallinity, this reaction was further optimized in Pyrex tubes regarding synthesis time (1 – 4 h) and M:H_2L ratios. The temperature was set to 120 °C and the metal to linker ratios 1:1 and 1:2 were used. According to the PXRD data highly crystalline products are already obtained after 1 h and 3 h using a molar ratio of M : L = 1:2 and 1:1, respectively (Fig. S2.2.). For further investigations a molar ration M:L = of 1:1 was chosen.

Table S2.1. Reaction parameters of the HT-assisted synthesis optimisation of Zr-UiO-66-PDC (M = metal source, L = H_2PDC, HCOOH = formic acid). The red box indicates the optimized reaction parameters for the synthesis of Zr-UiO-66-PDC with $Zr(SO_4)_2\cdot4H_2O$ as metal source.

M : L	Metal source	M / mg	H_2PDC / mg	H_2O / µL	HCOOH / µL
1 : 3	$Zr(SO_4)_2\cdot4H_2O$	35.5	50.1	450	550
1 : 3	$Zr(SO_4)_2\cdot4H_2O$	35.5	50.1	400	600
1 : 3	$Zr(SO_4)_2\cdot4H_2O$	35.5	50.1	350	650
1 : 3	$Zr(SO_4)_2\cdot4H_2O$	35.5	50.1	300	700
1 : 3	$Zr(SO_4)_2\cdot4H_2O$	35.5	50.1	250	750
1 : 3	$Zr(SO_4)_2\cdot4H_2O$	35.5	50.1	200	800
1 : 3	$Zr(SO_4)_2\cdot4H_2O$	35.5	50.1	150	850
1 : 3	$Zr(SO_4)_2\cdot4H_2O$	35.5	50.1	100	900
1 : 3	$Zr(SO_4)_2\cdot4H_2O$	35.5	50.1	50	950
1 : 2	$Zr(SO_4)_2\cdot4H_2O$	35.5	33.4	450	550
1 : 2	$Zr(SO_4)_2\cdot4H_2O$	35.5	33.4	400	600
1 : 2	$Zr(SO_4)_2\cdot4H_2O$	35.5	33.4	350	650
1 : 2	$Zr(SO_4)_2\cdot4H_2O$	35.5	33.4	300	700
1 : 2	$Zr(SO_4)_2\cdot4H_2O$	35.5	33.4	250	750
1 : 2	$Zr(SO_4)_2\cdot4H_2O$	35.5	33.4	200	800
1 : 2	$Zr(SO_4)_2\cdot4H_2O$	35.5	33.4	150	850
1 : 2	$Zr(SO_4)_2\cdot4H_2O$	35.5	33.4	100	900
1 : 2	$Zr(SO_4)_2\cdot4H_2O$	35.5	33.4	50	950
1 : 1	$Zr(SO_4)_2\cdot4H_2O$	35.5	16.7	600	400
1 : 1	$Zr(SO_4)_2\cdot4H_2O$	35.5	16.7	500	500
1 : 1	$Zr(SO_4)_2\cdot4H_2O$	35.5	16.7	250	750

Table S2.2. Reaction parameters of the HT-assisted synthesis of Zr-UiO-66-PDC (M = metal source, L = H_2PDC, HCOOH = formic acid). The red box indicates the optimized reaction parameters for the synthesis of Zr-UiO-66-PDC with $ZrOCl_2{\cdot}8H_2O$ as metal source.

M : L	Metal source	M / g	H_2PDC / g	H_2O / µL	HCOOH / µL
1 : 2	$ZrOCl_2{\cdot}8H_2O$	0.0322	0.0334	900	100
1 : 2	$ZrOCl_2{\cdot}8H_2O$	0.0322	0.0334	800	200
1 : 2	$ZrOCl_2{\cdot}8H_2O$	0.0322	0.0334	700	300
1 : 2	$ZrOCl_2{\cdot}8H_2O$	0.0322	0.0334	600	400
1 : 2	$ZrOCl_2{\cdot}8H_2O$	0.0322	0.0334	500	500
1 : 2	$ZrOCl_2{\cdot}8H_2O$	0.0322	0.0334	400	600
1 : 2	$ZrOCl_2{\cdot}8H_2O$	0.0322	0.0334	350	650
1 : 2	$ZrOCl_2{\cdot}8H_2O$	0.0322	0.0334	300	700
1 : 2	$ZrOCl_2{\cdot}8H_2O$	0.0322	0.0334	200	800
1 : 2	$ZrOCl_2{\cdot}8H_2O$	0.0322	0.0334	150	850
1 : 2	$ZrOCl_2{\cdot}8H_2O$	0.0322	0.0334	100	900
1 : 2	$ZrOCl_2{\cdot}8H_2O$	0.0322	0.0334	50	950
1 : 1	$ZrOCl_2{\cdot}8H_2O$	0.0322	0.0167	350	650
1 : 1	$ZrOCl_2{\cdot}8H_2O$	0.0322	0.0167	300	700
1 : 1	$ZrOCl_2{\cdot}8H_2O$	0.0322	0.0167	200	800
1 : 1	$ZrOCl_2{\cdot}8H_2O$	0.0322	0.0167	150	850
1 : 1	$ZrOCl_2{\cdot}8H_2O$	0.0322	0.0167	100	900
1 : 1	$ZrOCl_2{\cdot}8H_2O$	0.0322	0.0167	50	950

Table S2.3. Reaction parameters of the HT-assisted synthesis of Zr-UiO-66-PDC (M = metal source, L = H_2PDC, HCOOH = formic acid). The red box indicates the optimized reaction parameters for the synthesis of Zr-UiO-66-PDC with $ZrCl_4$ as metal source.

M : L	Metal source	M / g	H_2PDC / g	H_2O / µL	HCOOH / µL
1 : 2	$ZrCl_4$	0.0233	0.0334	350	650
1 : 2	$ZrCl_4$	0.0233	0.0334	300	700
1 : 2	$ZrCl_4$	0.0233	0.0334	200	800
1 : 2	$ZrCl_4$	0.0233	0.0334	150	850
1 : 2	$ZrCl_4$	0.0233	0.0334	100	900
1 : 2	$ZrCl_4$	0.0233	0.0334	50	950

Table S2.4. Reaction parameters of the HT-assisted synthesis of Zr-UiO-66-PDC (M = metal source, L = H_2PDC, HCOOH = formic acid). The red box indicates the optimized reaction parameters for the synthesis of Zr-UiO-66-PDC with $Zr(CO_3)_2$ as metal source.

M : L	Metal source	M / g	H_2PDC / g	H_2O / µL	HCOOH / µL
1 : 2	$Zr(CO_3)_2$	0.0211	0.0334	350	650
1 : 2	$Zr(CO_3)_2$	0.0211	0.0334	300	700
1 : 2	$Zr(CO_3)_2$	0.0211	0.0334	200	800
1 : 2	$Zr(CO_3)_2$	0.0211	0.0334	150	850
1 : 2	$Zr(CO_3)_2$	0.0211	0.0334	100	900
1 : 2	$Zr(CO_3)_2$	0.0211	0.0334	50	950
1 : 1	$Zr(CO_3)_2$	0.0211	0.0167	350	650
1 : 1	$Zr(CO_3)_2$	0.0211	0.0167	300	700
1 : 1	$Zr(CO_3)_2$	0.0211	0.0167	200	800
1 : 1	$Zr(CO_3)_2$	0.0211	0.0167	150	850
1 : 1	$Zr(CO_3)_2$	0.0211	0.0167	100	900
1 : 1	$Zr(CO_3)_2$	0.0211	0.0167	50	950

Table S2.5. Reaction parameters of the HT-assisted synthesis of Zr-UiO-66-PDC (M = metal source, L = H_2PDC, HCOOH = formic acid). The red box indicates the optimized reaction parameters for the synthesis of Zr-UiO-66-PDC with $ZrO(NO_3)_2 \cdot xH_2O$ as metal source.

M : L	Metal source	M / g	H_2PDC / g	H_2O / µL	HCOOH / µL
1 : 2	$ZrO(NO_3)_2 \cdot xH_2O$	0.0231	0.0334	350	650
1 : 2	$ZrO(NO_3)_2 \cdot xH_2O$	0.0231	0.0334	300	700
1 : 2	$ZrO(NO_3)_2 \cdot xH_2O$	0.0231	0.0334	200	800
1 : 2	$ZrO(NO_3)_2 \cdot xH_2O$	0.0231	0.0334	150	850
1 : 2	$ZrO(NO_3)_2 \cdot xH_2O$	0.0231	0.0334	100	900
1 : 2	$ZrO(NO_3)_2 \cdot xH_2O$	0.0231	0.0334	50	950

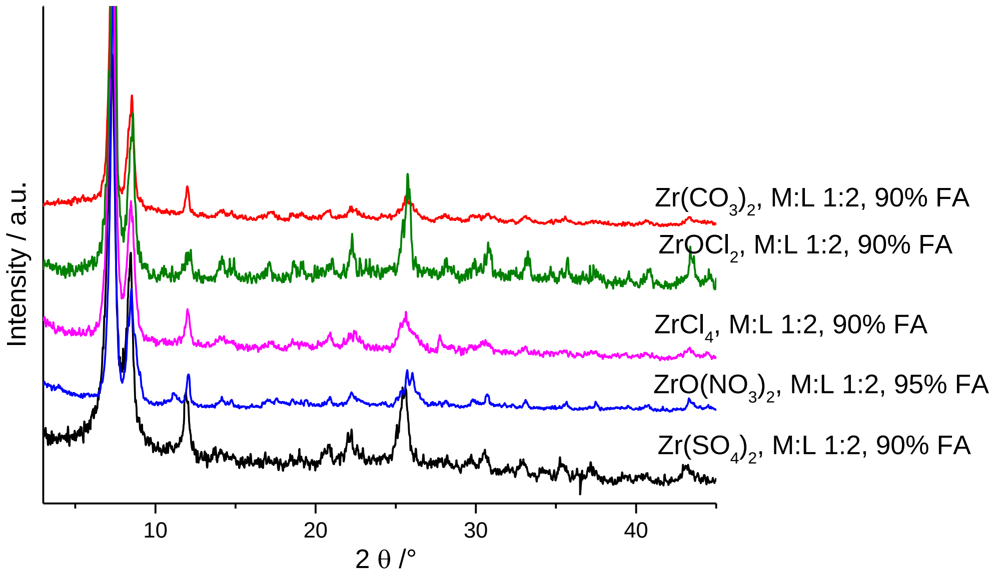

Fig. S2.1. PXRD patterns of the Zr-UiO-66-PDC products obtained using different Zr-salts and the respectively optimized reaction conditions ($CuK_{\alpha 1}$ radiation).

Table S2.6. Reaction time optimization of the optimized synthesis conditions for Zr-UiO-66-PDC with $ZrOCl_2$ varied in Pyrex tubes (M = metal source, L = H_2PDC, HCOOH = formic acid). The red box shows the optimized reaction parameters for the synthesis of Zr-UiO-66-PDC.

M : L	Metal source	M / g	H_2PDC / g	H_2O / µL	HCOOH / µL	T / °C	t / h
1 : 1	$ZrOCl_2·8H_2O$	0.0856	0.044	300	2700	120	1
1 : 1	$ZrOCl_2·8H_2O$	0.0856	0.044	300	2700	120	2
1 : 1	$ZrOCl_2·8H_2O$	0.0856	0.044	300	2700	120	3
1 : 1	$ZrOCl_2·8H_2O$	0.0856	0.044	300	2700	120	4
1 : 2	$ZrOCl_2·8H_2O$	0.0856	0.088	300	2700	120	1
1 : 2	$ZrOCl_2·8H_2O$	0.0856	0.088	300	2700	120	2
1 : 2	$ZrOCl_2·8H_2O$	0.0856	0.088	300	2700	120	3
1 : 2	$ZrOCl_2·8H_2O$	0.0856	0.088	300	2700	120	4

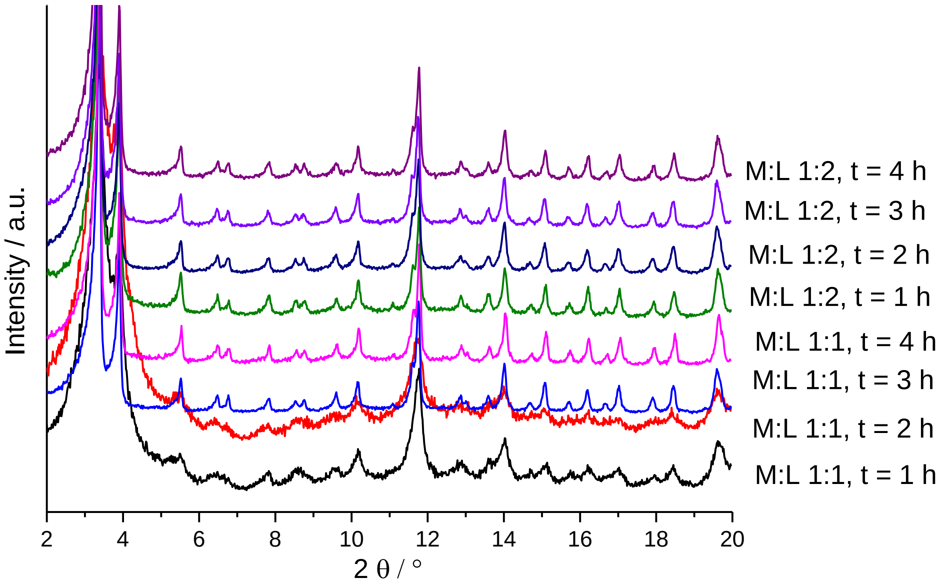

Fig. S2.2. PXRD patterns of the Zr-UiO-66-PDC products obtained using $ZrOCl_2·8H_2O$ as Zr-salt, formic acid as modulator with two different metal to linker ratios and temperatures from one to four hours (MoK$_{\alpha 1}$ radiation).

S3 Discovery, Optimization and Synthesis of Hf-UiO-66-PDC

The systematic investigation of the synthesis of Zr-UiO-66-PDC showed that the product could not be obtained in DMF or DMF/solvent mixtures. Thus for Hf-UiO-66-PDC every reaction was carried out in water with $HfCl_4$ as metal salt. In the high throughput investigation different metal to linker ratios (2:1, 1:1, 1:2), different modulators (formic acid, acetic acid and hydrochloric acid) and different water to modulator ratios were tested. (Table S3.1. to Table S.3.3.). The reaction time was 24 h and the reaction temperature was 120 °C for every reaction. The optimized metal to linker ratio is 1:1 with similar water to modulator ratios for all different modulators. PXRD pattern of the optimized reactions are shown in Fig.S.3.1. Reaction time and temperature optimization were carried out with the optimized synthesis utilising acetic acid as modulator in pyrex tubes (Table S3.4.), the PXRD patterns are shown in Fig S.3.2.

Table S3.1. Reaction parameters of the HT-assisted synthesis of Hf-UiO-66-PDC (M = metal source, L = H_2PDC, HCOOH = formic acid). The red box indicates the optimized reaction parameters for the synthesis of Hf-UiO-66-PDC with formic acid as modulator.

M : L	Metal source	M / g	H_2PDC / g	H_2O / µL	HCOOH / µL
1 : 2	$HfCl_4$	0.0320	0.0334	1000	0
1 : 2	$HfCl_4$	0.0320	0.0334	900	100
1 : 2	$HfCl_4$	0.0320	0.0334	800	200
1 : 2	$HfCl_4$	0.0320	0.0334	700	300
1 : 2	$HfCl_4$	0.0320	0.0334	600	400
1 : 2	$HfCl_4$	0.0320	0.0334	500	500
1 : 2	$HfCl_4$	0.0320	0.0334	400	600
1 : 2	$HfCl_4$	0.0320	0.0334	300	700
1 : 2	$HfCl_4$	0.0320	0.0334	200	800
1 : 2	$HfCl_4$	0.0320	0.0334	100	900
1 : 2	$HfCl_4$	0.0320	0.0334	0	1000
1 : 1	$HfCl_4$	0.0320	0.0167	1000	0
1 : 1	$HfCl_4$	0.0320	0.0167	900	100
1 : 1	$HfCl_4$	0.0320	0.0167	800	200
1 : 1	$HfCl_4$	0.0320	0.0167	700	300
1 : 1	$HfCl_4$	0.0320	0.0167	600	400
1 : 1	$HfCl_4$	0.0320	0.0167	500	500
1 : 1	$HfCl_4$	0.0320	0.0167	400	600
1 : 1	$HfCl_4$	0.0320	0.0167	300	700
1 : 1	$HfCl_4$	0.0320	0.0167	200	800
1 : 1	$HfCl_4$	0.0320	0.0167	100	900
1 : 1	$HfCl_4$	0.0320	0.0167	0	1000
2 : 1	$HfCl_4$	0.0641	0.0167	1000	0
2 : 1	$HfCl_4$	0.0641	0.0167	900	100
2 : 1	$HfCl_4$	0.0641	0.0167	800	200
2 : 1	$HfCl_4$	0.0641	0.0167	700	300
2 : 1	$HfCl_4$	0.0641	0.0167	600	400
2 : 1	$HfCl_4$	0.0641	0.0167	500	500
2 : 1	$HfCl_4$	0.0641	0.0167	400	600
2 : 1	$HfCl_4$	0.0641	0.0167	300	700
2 : 1	$HfCl_4$	0.0641	0.0167	200	800

2 : 1	$HfCl_4$	0.0641	0.0167	100	900
2 : 1	$HfCl_4$	0.0641	0.0167	0	1000

Table S3.2. Reaction parameters of the HT-assisted synthesis of Hf-UiO-66-PDC (M = metal source, L = H_2PDC, CH_3COOH = acetic acid). The red box indicates the optimized reaction parameters for the synthesis of Hf-UiO-66-PDC with acetic acid as modulator.

M : L	Metal source	M / g	H_2PDC / g	H_2O / µL	CH_3COOH / µL
1 : 2	$HfCl_4$	0.0320	0.0334	1000	0
1 : 2	$HfCl_4$	0.0320	0.0334	900	100
1 : 2	$HfCl_4$	0.0320	0.0334	800	200
1 : 2	$HfCl_4$	0.0320	0.0334	700	300
1 : 2	$HfCl_4$	0.0320	0.0334	600	400
1 : 2	$HfCl_4$	0.0320	0.0334	500	500
1 : 2	$HfCl_4$	0.0320	0.0334	400	600
1 : 2	$HfCl_4$	0.0320	0.0334	300	700
1 : 2	$HfCl_4$	0.0320	0.0334	200	800
1 : 2	$HfCl_4$	0.0320	0.0334	100	900
1 : 2	$HfCl_4$	0.0320	0.0334	0	1000
1 : 1	$HfCl_4$	0.0320	0.0167	1000	0
1 : 1	$HfCl_4$	0.0320	0.0167	900	100
1 : 1	$HfCl_4$	0.0320	0.0167	800	200
1 : 1	$HfCl_4$	0.0320	0.0167	700	300
1 : 1	$HfCl_4$	0.0320	0.0167	600	400
1 : 1	$HfCl_4$	0.0320	0.0167	500	500
1 : 1	$HfCl_4$	0.0320	0.0167	400	600
1 : 1	$HfCl_4$	0.0320	0.0167	300	700
1 : 1	$HfCl_4$	0.0320	0.0167	200	800
1 : 1	$HfCl_4$	0.0320	0.0167	100	900
1 : 1	$HfCl_4$	0.0320	0.0167	0	1000
2 : 1	$HfCl_4$	0.0641	0.0167	1000	0
2 : 1	$HfCl_4$	0.0641	0.0167	900	100
2 : 1	$HfCl_4$	0.0641	0.0167	800	200
2 : 1	$HfCl_4$	0.0641	0.0167	700	300
2 : 1	$HfCl_4$	0.0641	0.0167	600	400
2 : 1	$HfCl_4$	0.0641	0.0167	500	500
2 : 1	$HfCl_4$	0.0641	0.0167	400	600
2 : 1	$HfCl_4$	0.0641	0.0167	300	700
2 : 1	$HfCl_4$	0.0641	0.0167	200	800
2 : 1	$HfCl_4$	0.0641	0.0167	100	900
2 : 1	$HfCl_4$	0.0641	0.0167	0	1000

Table S3.3. Reaction parameters of the HT-assisted synthesis of Hf-UiO-66-PDC (M = metal source, L = H_2PDC, HCl = hydrochloric acid). The red box indicates the optimized reaction parameters for the synthesis of Hf-UiO-66-PDC with HCl as modulator.

M : L	Metal source	M / g	H_2PDC / g	H_2O / µL	HCl / µL
1 : 2	$HfCl_4$	0.0320	0.0334	1000	0
1 : 2	$HfCl_4$	0.0320	0.0334	900	100
1 : 2	$HfCl_4$	0.0320	0.0334	800	200
1 : 2	$HfCl_4$	0.0320	0.0334	700	300
1 : 2	$HfCl_4$	0.0320	0.0334	600	400
1 : 2	$HfCl_4$	0.0320	0.0334	500	500
1 : 2	$HfCl_4$	0.0320	0.0334	400	600
1 : 2	$HfCl_4$	0.0320	0.0334	300	700
1 : 2	$HfCl_4$	0.0320	0.0334	200	800
1 : 2	$HfCl_4$	0.0320	0.0334	100	900
1 : 2	$HfCl_4$	0.0320	0.0334	0	1000
1 : 1	$HfCl_4$	0.0320	0.0167	1000	0
1 : 1	$HfCl_4$	0.0320	0.0167	900	100
1 : 1	$HfCl_4$	0.0320	0.0167	800	200
1 : 1	$HfCl_4$	0.0320	0.0167	700	300
1 : 1	$HfCl_4$	0.0320	0.0167	600	400
1 : 1	$HfCl_4$	0.0320	0.0167	500	500
1 : 1	$HfCl_4$	0.0320	0.0167	400	600
1 : 1	$HfCl_4$	0.0320	0.0167	300	700
1 : 1	$HfCl_4$	0.0320	0.0167	200	800
1 : 1	$HfCl_4$	0.0320	0.0167	100	900
1 : 1	$HfCl_4$	0.0320	0.0167	0	1000
2 : 1	$HfCl_4$	0.0641	0.0167	1000	0
2 : 1	$HfCl_4$	0.0641	0.0167	900	100
2 : 1	$HfCl_4$	0.0641	0.0167	800	200
2 : 1	$HfCl_4$	0.0641	0.0167	700	300
2 : 1	$HfCl_4$	0.0641	0.0167	600	400
2 : 1	$HfCl_4$	0.0641	0.0167	500	500
2 : 1	$HfCl_4$	0.0641	0.0167	400	600
2 : 1	$HfCl_4$	0.0641	0.0167	300	700
2 : 1	$HfCl_4$	0.0641	0.0167	200	800
2 : 1	$HfCl_4$	0.0641	0.0167	100	900
2 : 1	$HfCl_4$	0.0641	0.0167	0	1000

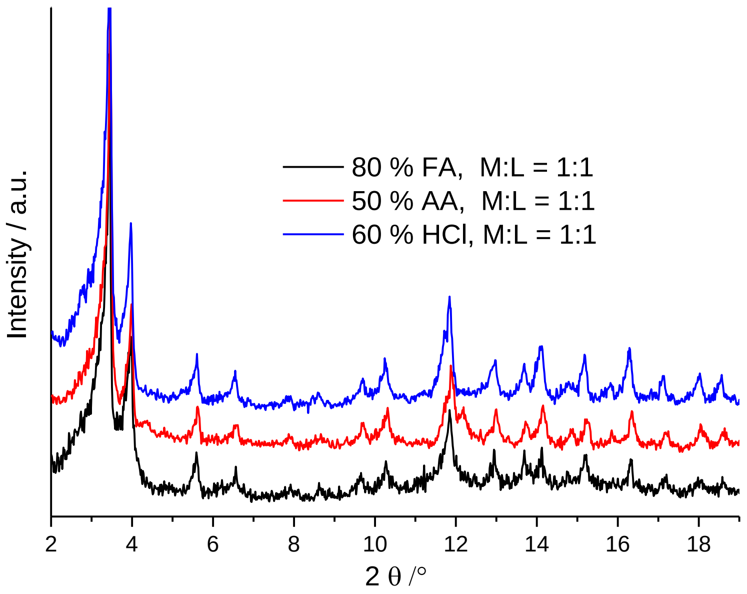

Fig. S3.1. PXRD patterns of the Hf-UiO-66-PDC products obtained using different modulators and the respectively optimized reaction conditions (MoK$_{\alpha 1}$ radiation).

Table S.3.4. Reaction time and temperature optimization for the synthesis of Hf-UiO-66-PDC with acetic acid as modulator varied in Pyrex tubes (M = metal source, L = H_2PDC, AA = acetic acid). The red box shows the optimized reaction parameter for the synthesis of Hf-UiO-66-PDC.

M : L	Metal source	M / g	H_2PDC / g	H_2O / µL	AA / µL	T / °C	t / min
1 : 1	$HfCl_4$	0.096	0.0501	1500	1500	100	20
1 : 1	$HfCl_4$	0.096	0.0501	1500	1500	100	60
1 : 1	$HfCl_4$	0.096	0.0501	1500	1500	100	80
1 : 1	$HfCl_4$	0.096	0.0501	1500	1500	120	20
1 : 1	$HfCl_4$	0.096	0.0501	1500	1500	120	40
1 : 1	$HfCl_4$	0.096	0.0501	1500	1500	120	60

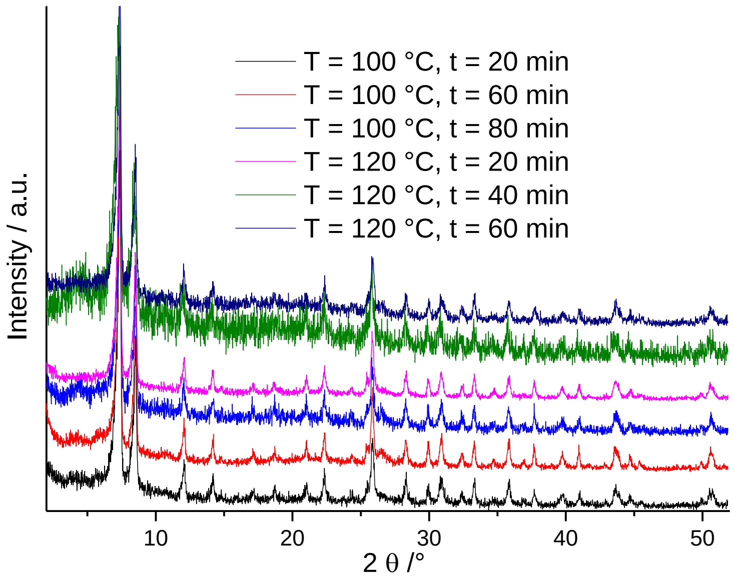

Fig. S3.2. PXRD patterns of the Hf-UiO-66-PDC products obtained using acetic acid as modulator, different reaction temperatures (100 and 120 °C) and reactions times (20 to 60 min) (CuK$_{\alpha 1}$ radiation).

S4 Discovery, Optimization and Synthesis of Ce-UiO-66-PDC

The reaction time of the synthesis of Ce-UiO-66-PDC was optimized in Pyrex tubes with a reaction temperature of 90 °C (Table S4.1.), the powder patterns are shown in Fig S.4.1.

Table S4.1. Reaction parameters of reaction time optimization of the synthesis of Ce-UiO-66-PDC (M = metal source, L = H_2PDC, HNO_3 = conc. nitric acid). The red box shows the optimized reaction parameters for the synthesis of Ce-UiO-66-PDC.

M : L	Metal source	M / g	H_2PDC / g	H_2O / µL	HNO_3 / µL	t / min
1 : 1	$(NH_4)_2[Ce(NO_3)_6]$	0.660	0.167	3000	500	15
1 : 1	$(NH_4)_2[Ce(NO_3)_6]$	0.660	0.167	3000	500	30
1 : 1	$(NH_4)_2[Ce(NO_3)_6]$	0.660	0.167	3000	500	45
1 : 1	$(NH_4)_2[Ce(NO_3)_6]$	0.660	0.167	3000	500	60

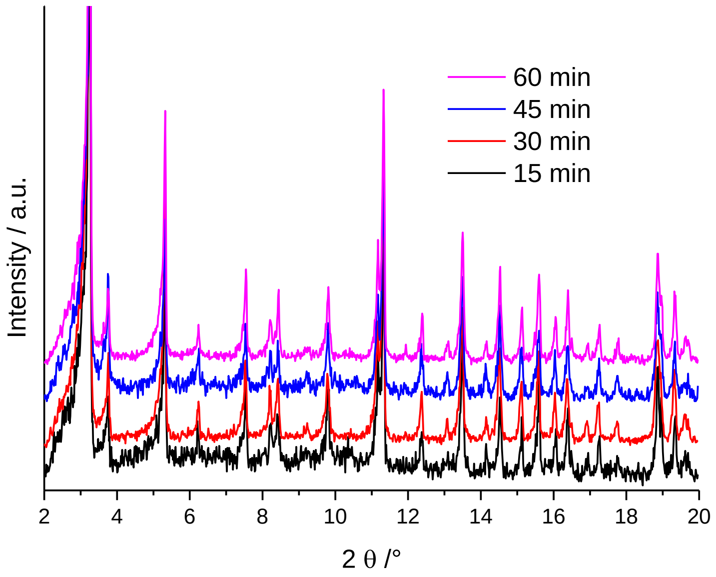

Fig. S4.1. PXRD patterns of the Ce-UiO-66-PDC products obtained using $(NH_4)_2[Ce(NO_3)_6]$ as metal source, conc. nitric acid as modulator and different reactions times (15 to 60 min) (MoK$_{\alpha1}$ radiation).

S5 Structural Analysis of M-UiO-66-PDC (M = Zr, Ce, Hf)

S5.1 Details of the Rietveld Refinement using fixed occupancies of the linker

Laboratory powder X-ray diffraction data were collected in transmission geometry using a Stoe Stadi P diffractometer fitted with a Cu $K_{\alpha1}$ tube radiation source and a Mythen detector. All stages of the refinement were performed using the routines of TOPAS-Academic V5.[1]

For the refinement of the PXRD pattern of **Zr-UiO-66-PDC**, the structure of Zr-UiO-66-BDC was directly used, only accounting for the fractional occupation of the lateral atoms by nitrogen. Moreover the total occupancy for the atoms forming the linker molecule was fixed to 83.3 % being in agreement with five linker molecules per cluster as observed in the TG experiments. It is noted that due to the presence of guest molecules in the MOF, which are modeled as ordered atoms, the occupancy of the linkers cannot be freely refined. The results show that the structural model can describe the data.

For **Ce-UiO-66-PDC**, the pattern is in agreement with the cubic symmetry of the UiO-66 framework. Thus, a starting model for the refinement was developed by replacing the Zr atoms in UiO-66-BDC by Ce atoms and defining the lateral atoms of the aromatic ring as partially occupied by carbon (75 %) and nitrogen atoms (25%). Subsequently this model was fully refined by Rietveld methods. The overall occupancy of the linker molecules was fixed to 1, being in agreement with the results of the TG experiments. Similarly the model for **Hf-UiO-66-PDC** was generated, replacing Zr by Hf atoms. However, the overall occupancy for the linker molecules was fixed to 66 %, being in agreement with the results of the TG experiments. The additional broad peaks are due to the presence of **reo** domains in the particles and were ignored for the refinement. Residual electron density inside the pores was attributed to oxygen atoms representing guest molecules in all these structures. The results show that the structural model can describe the data.

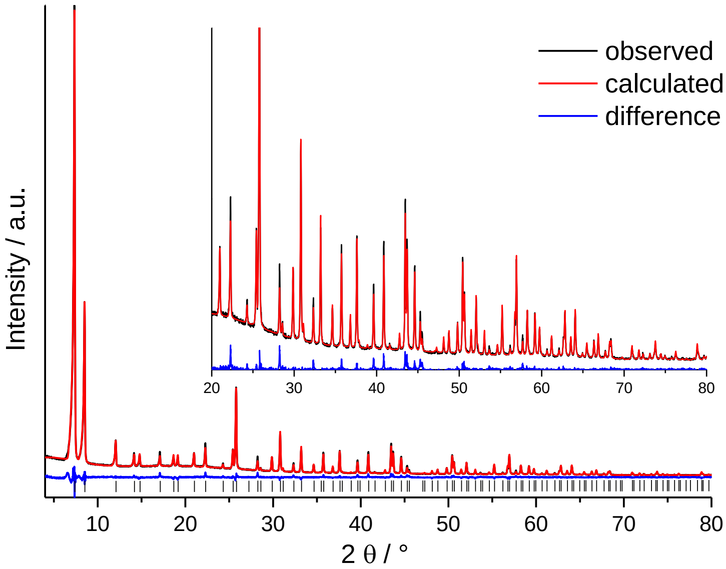

Fig. S5.1. Rietveld plot for the final refinement of Zr-UiO-66-PDC using a fixed occupancy factor for the linker molecule. Black line gives the experimental data, red line the calculated fit and the blue line is the difference curve. Black bars indicate the Bragg reflection positions.

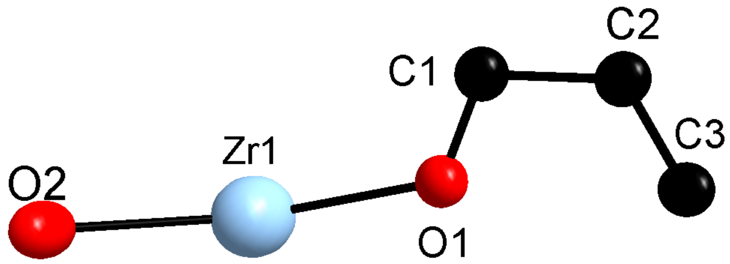

Fig. S5.2. Asymmetric unit of Zr-UiO-66-PDC. Oxygen atoms representing water molecules are omitted for clarity.

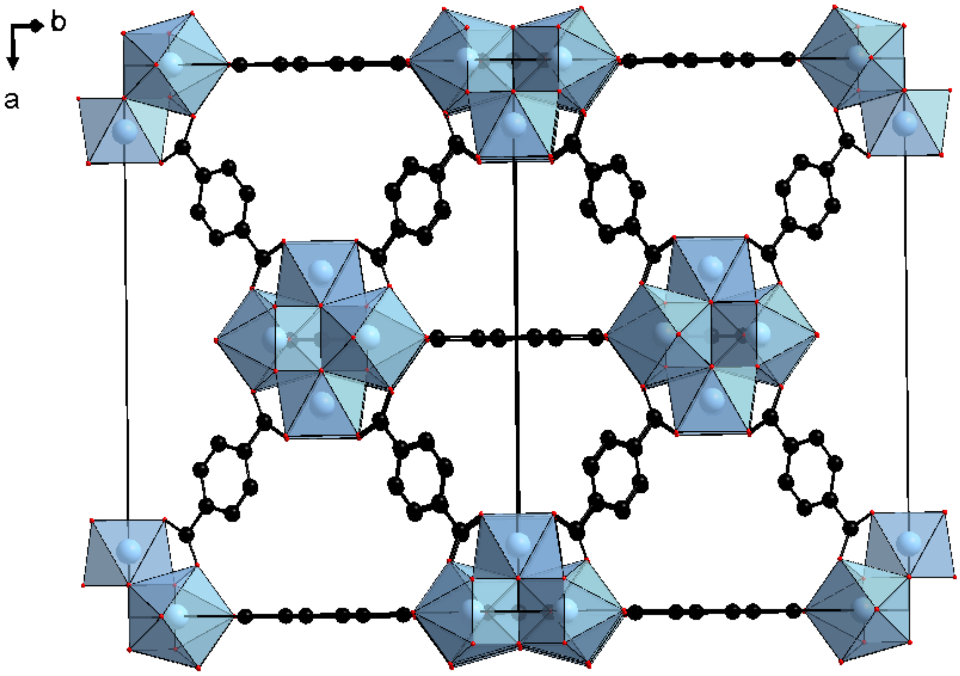

Fig. S5.3. Unit cell of Zr-UiO-66-PDC. Oxygen atoms representing water molecules are omitted for clarity.

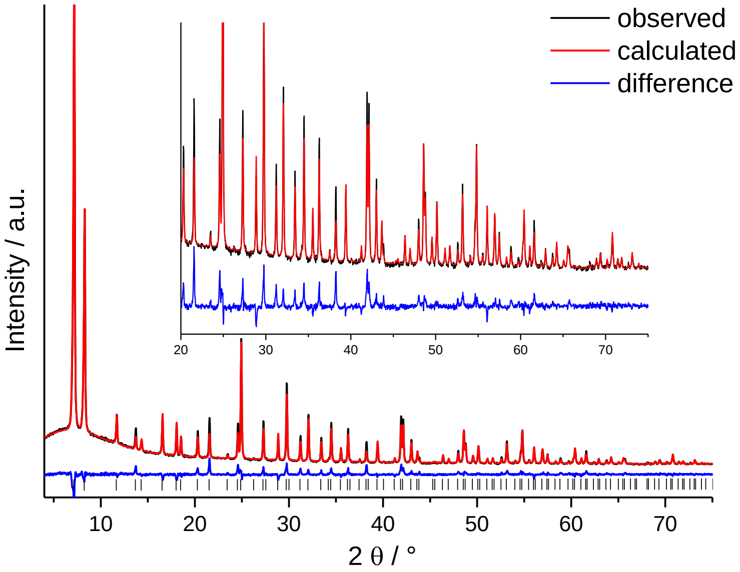

Fig. S5.4. Rietveld plot for the final refinement of Ce-UiO-66-PDC using a fixed occupancy factor for the linker molecule. Black line gives the experimental data, red line the calculated fit and the blue line is the difference curve. Black bars indicate the Bragg reflection positions.

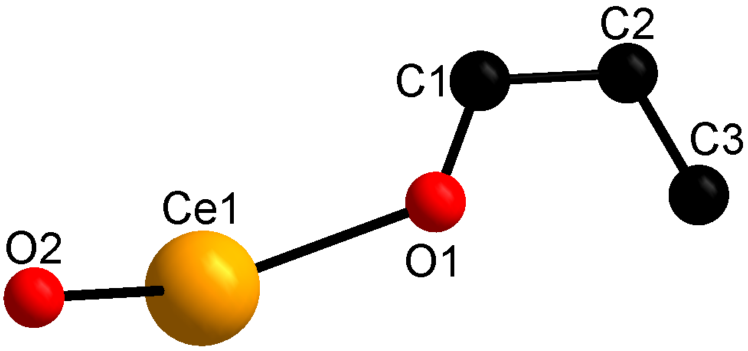

Fig. S5.5. Asymmetric unit of Ce-UiO-66-PDC. Oxygen atoms representing water molecules are omitted for clarity.

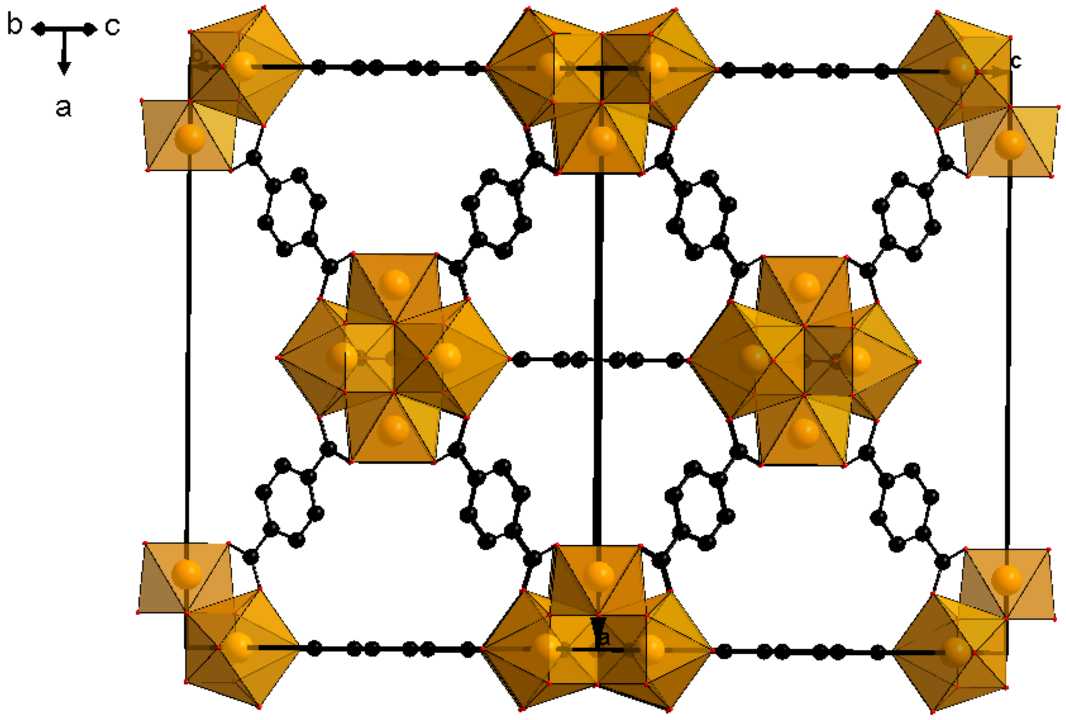

Fig. S5.6. Unit cell of Ce-UiO-66-PDC. Oxygen atoms representing water molecules are omitted for clarity.

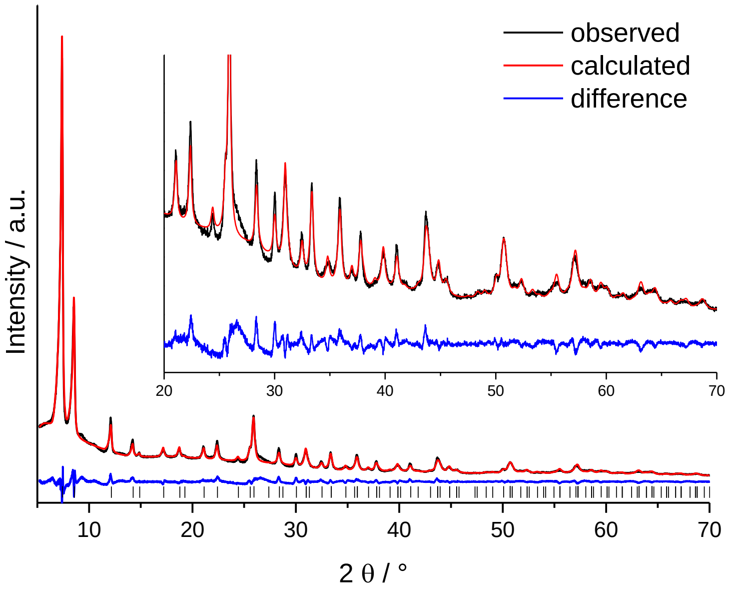

Fig. S5.7. Rietveld plot for the final refinement of Hf-UiO-66-PDC using a fixed occupancy factor for the linker molecule. Black line gives the experimental data, red line the calculated fit and the blue line is the difference curve. Black bars indicate the Bragg reflection positions.

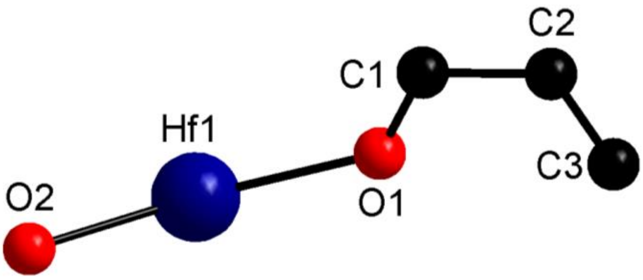

Fig. S5.8. Asymmetric unit of Hf-UiO-66-PDC. Oxygen atoms representing water molecules are omitted for clarity.

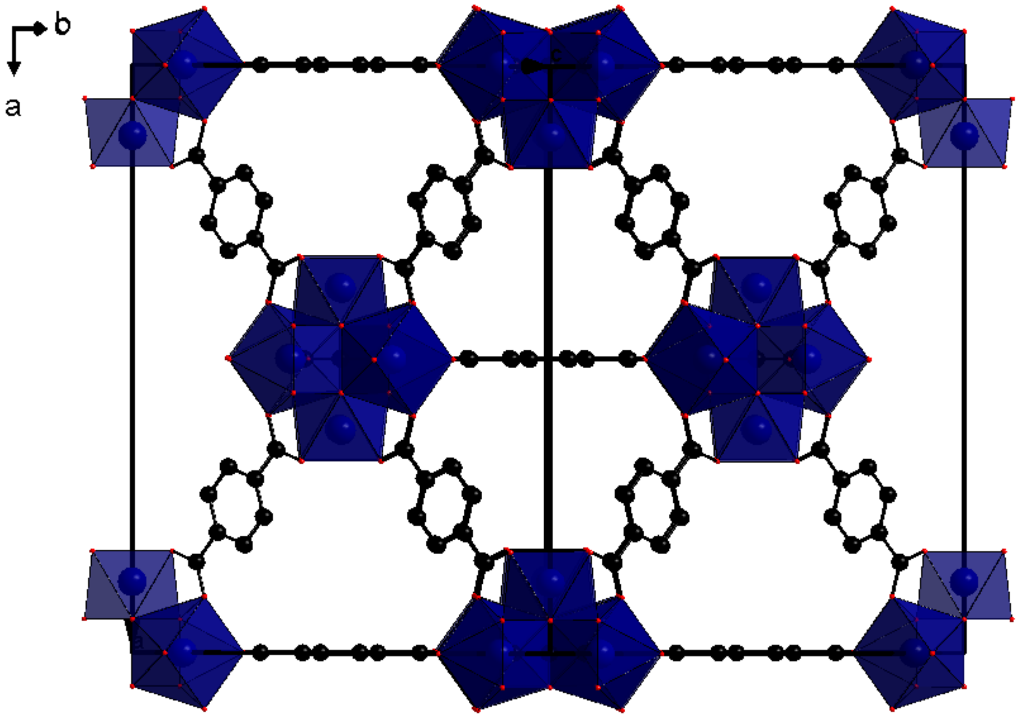

Fig. S5.9. Unit cell of Hf-UiO-66-PDC. Oxygen atoms representing water molecules are omitted for clarity.

Table S5.1. Crystallographic data for M-UiO-66-PDC (M = Zr, Ce, Hf).

Compound	Zr-UiO-66-PDC	Ce-UiO-66-PDC	Hf-UiO-66-PDC
Space Group	*Fm*-3*m*	*Fm*-3*m*	*Fm*-3*m*
Crystal System	Cubic	Cubic	Cubic
a / Å	20.6819(1)	21.4579(2)	20.5847(8)
b / Å	20.6819(1)	21.4579(2)	20.5847(8)
c / Å	20.6819(1)	21.4579(2)	20.5847(8)
α / °	90	90	90
β / °	90	90	90
γ / °	90	90	90
V / Å^3	8846.5(1)	9880.1(3)	8722(1)
Wavelength	Cu K$_{\alpha1}$	Cu K$_{\alpha1}$	Cu K$_{\alpha1}$
R$_p$ / %	3.6	3.9	3.8
R$_{wp}$ / %	4.9	5.6	5.0
GoF	1.3	2.1	2.3
R$_{Bragg}$ / %	2.2	5.3	1.9

Table S5.2. Comparison of the figures of merit from the Rietveld refinement using the defective model as derived from the results of the other characterisation methods and using a defect-free (ideal) UiO-66-type frameworks.

	Zr-UiO-66-PDC		Hf-UiO-66-PDC	
	defective	ideal	defective	ideal
Ratio M^{4+}:Linker	6:5	6:6	6:4	6:6
R$_P$	3.6	4.1	3.8	4.4
R$_{WP}$	4.9	5.9	5.0	5.8
GoF	1.3	1.6	2.3	2.7
R$_{Bragg}$	2.2	2.9	1.9	3.0

S5.2 Zr-UiO-66-PDC Zr K-edge EXAFS data treatment

Preliminary EXAFS data treatment (background subtraction, normalization, averaging) was carried out using the Athena code, while subsequent fitting was made using the Artemis code, both programs being part of Demeter package.[2] The fit was performed in R-space considering k^3-weighted data. Results of the fit are presented in the Fig. S5.10.

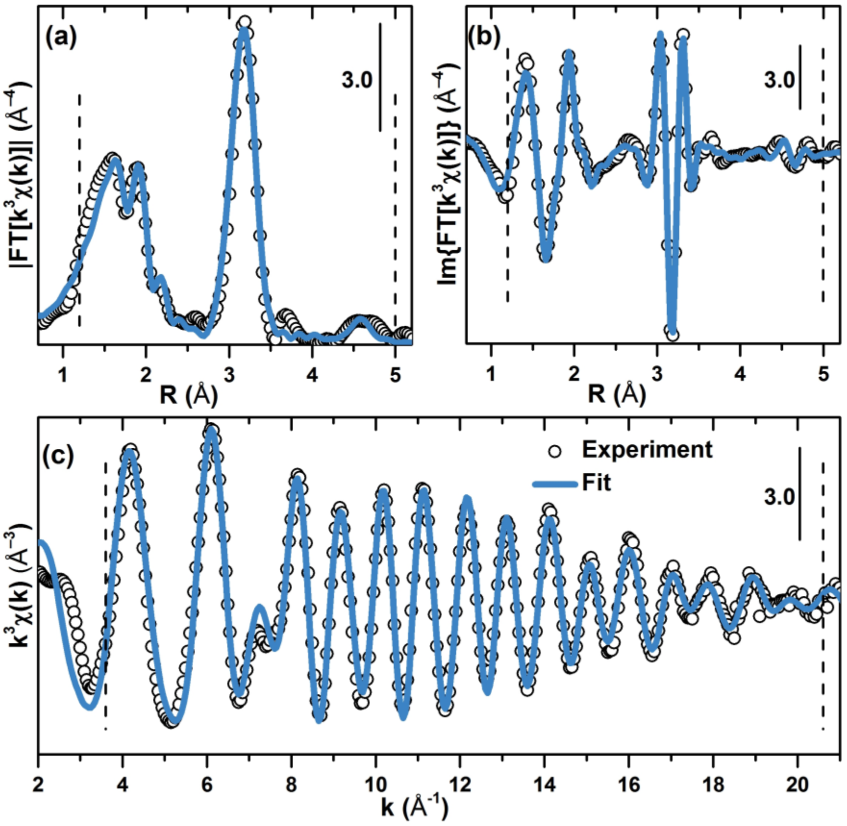

Fig. S5.10. Experimental Zr K-edge EXAFS data for Zr-UiO-66-PDC MOF compared to the fit: modulus (a) and imaginary part (b) of the k^3-weighted phase-uncorrected FT together with the $k^3\chi(k)$ signal (c) Ranges employed for FT (3.7 – 20.6 Å^{-1} in k-space) and fitting (1.2 – 5.0 Å in R-space) are shown by the vertical dotted lines on the corresponding panels.

Fitting was performed using the corresponding XRD structure as a model to calculate phase shifts and scattering amplitudes by FEFF6 code.[3] In total 7 scattering paths were included in the fit: single scattering paths formed by μ_3-O, O1, C, Cl, Zr1 and Zr2 atoms and the most intense multiple scattering path formed by O1 and C atoms. 12 fitting parameters were used:

- Energy shift ΔE and amplitude reduction factor S_0^2 common for all paths
- Independent elongation/contraction parameters ΔR for each of the single-scattering paths apart from Zr2 (5 parameters in total)
- Independent Debye-Waller parameters σ^2 for each of the single-scattering paths apart from Zr2 (5 parameters in total).

No additional parameters were introduced to deal with Zr-O1-C and Zr-Zr2 paths. Instead, ΔR for these paths were expressed through geometrical relations obtained by solving corresponding triangles and using the parameters already introduced for the single scattering paths:

$$\Delta R_{Zr2} = \sqrt{2} \cdot \Delta R_{Zr1}$$

$$\Delta R_{O1-C} = \frac{1}{2}(\Delta R_{O1} + \Delta R_{C} + (-0.53\Delta R_{O1} + 0.79\Delta R_{C}))$$

Corresponding Debye-Waller factors were analogously expressed by those of the already parametrized paths:

$$\sigma_{Zr2}^2 = \sigma_{Zr1}^2 \sqrt{\frac{R_{Zr2}}{R_{Zr1}}}$$

$$\sigma_{O1-C}^2 = \sigma_{O1}^2 + \sigma_{C}^2$$

Besides, degeneracy of Zr–C path was decreased by 17% (from 4 to 3.3) to simulate the missisng linker defects, while the degeneracy of Zr-Cl path was set to the remaining 0.7. Indeed, XRD data indicate that each cornerstone is connected in average only by 10 linkers instead of 12, while previous studies report that Cl is likely to fill the coordinative vacancies created by missing linkers.[4]

Based on the adopted model, the fit showed good overall agreement with the experimental EXAFS data and physically reasonable values of the employed parameters. Obtained bond distances are in agreement with the presented XRD data for Zr-UiO-66-PDC MOF and previously published data for standard UiO-66,[5,6] thus complementing the structural characterization of the studied compound.

S5.3 Ce-UiO-66-PDC Ce L_3-edge XANES spectra

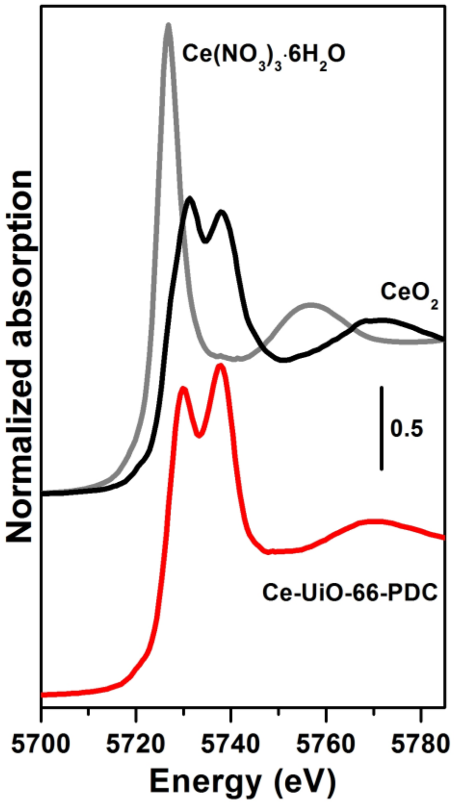

Fig. S5.11 Ce L_3-edge XANES spectrum of Ce-UiO-66-PDC MOF compared to Ce(IV) and Ce(III) reference compounds (CeO_2 and $Ce(NO_3)_3 \cdot 6H_2O$, respectively), proving the +4 oxidation state of Ce ions in the cornerstones of the MOF. Vertical shift is for the sake of clarity.

S6 NMR-Spectroscopy

Samples of M-UiO-66 with M = Zr, Ce and Hf were digested using a NaOD/D_2O solution and ^{1}H-NMR spectra were recorded to confirm or exclude the presence of modulator incorporated into the corresponding MOF (Fig.6.1. to Fig.6.3).

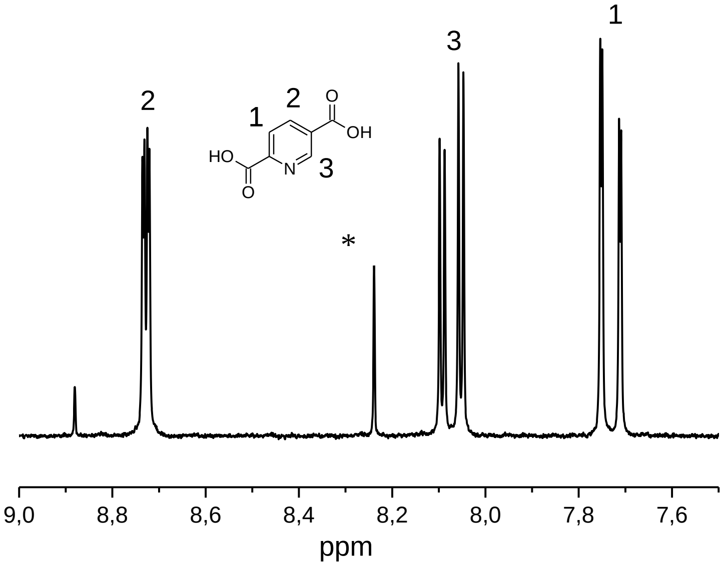

Fig. S6.1. ^{1}H-NMR-spectrum of Zr-UiO-66-PDC dissolved in NaOD/D_2O. * indicates a small amount of formate ions (< 0.5 per formula).

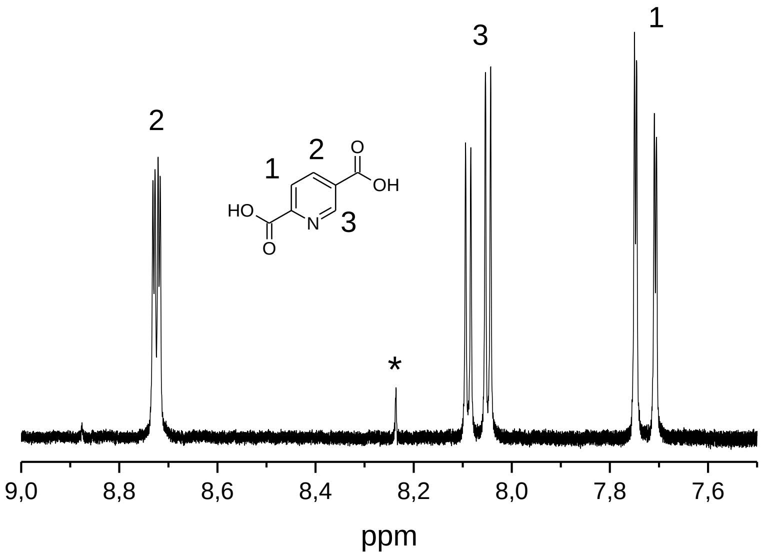

Fig. S6.2. ^{1}H-NMR-spectrum of Ce-UiO-66-PDC dissolved in NaOD/D_2O. * indicates a small amount of unknown impurity of about 2%. Since no formic acid was used in the synthesis we exclude the presence of formate ions in the structure of Ce-UiO-66-PDC.

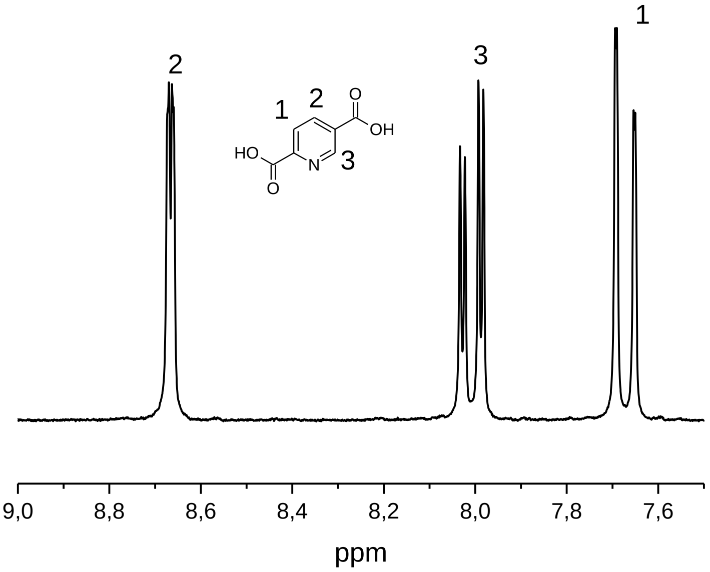

Fig. S6.3. ^{1}H-NMR-spectrum of Hf-UiO-66-PDC dissolved in NaOD/D_2O shows the absence of modulator in the product.

S7 Infrared Spectroscopy

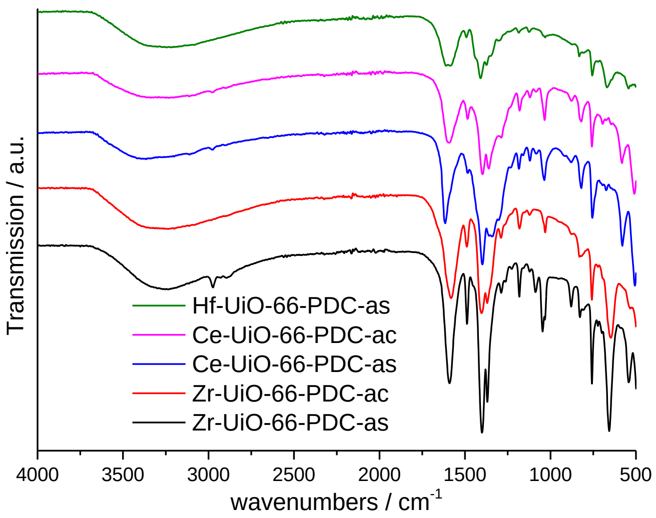

Fig. S7.1. FTIR spectra of the as synthesized (as) and the activated (ac) form of M-UiO-66-PDC with M = Zr, Ce, Hf.

Table S7.1. Assignment of the bands in the FTIR spectra of as synthesized (as) and the activated (ac) M-UiO-66-PDC with M = Zr, Ce, Hf.

MOF	Wavenumber / cm^{-1}	Intensity	Classification
Zr-UiO-66-PDC-as	2979	w	CH-stretch – $HCOO^{-}$
	1590	s	Asymmetric CO^{2-}stretch – PDC^{2-}
	1487	m	Symmetric CO^{2-}stretch – PDC^{2-}
	752, 659	s, s	2,5-disubstituted Pyridine
Zr-UiO-66-PDC-ac	1584	s	Asymmetric CO^{2-}stretch – PDC^{2-}
	1491	m	Symmetric CO^{2-}stretch – PDC^{2-}
	752, 650	s, s	2,5-disubstituted Pyridine
Ce-UiO-66-PDC-as	1616	s	Asymmetric CO^{2-}stretch – PDC^{2-}
	1484	w	Symmetric CO^{2-}stretch – PDC^{2-}
	819, 752	m	2,5-disubstituted Pyridine
Ce-UiO-66-PDC-ac	1594	s	Asymmetric CO^{2-}stretch – PDC^{2-}
	1484	m	Symmetric CO^{2-}stretch – PDC^{2-}
	820, 758	m, s	2,5-disubstituted Pyridine
Hf-UiO-66-PDC-as	1592	s	Asymmetric CO^{2-}stretch – PDC^{2-}
	1487	m	Symmetric CO^{2-}stretch – PDC^{2-}
	759, 660	s, s	2,5-disubstituted Pyridine

S9 Thermal and chemical stability

For the temperature depended PXRD measurements, the samples were prepared in 0.5 mm borosilicate capillaries, which were heated up to 300 °C. A PXRD pattern was measured every 5 °C for five minutes in transmission geometry using Mo $K_{\alpha1}$ radiation for Zr- and Ce-UiO-66-PDC. For Hf-UiO-66-PDC Cu $K_{\alpha1}$ radiation was used.

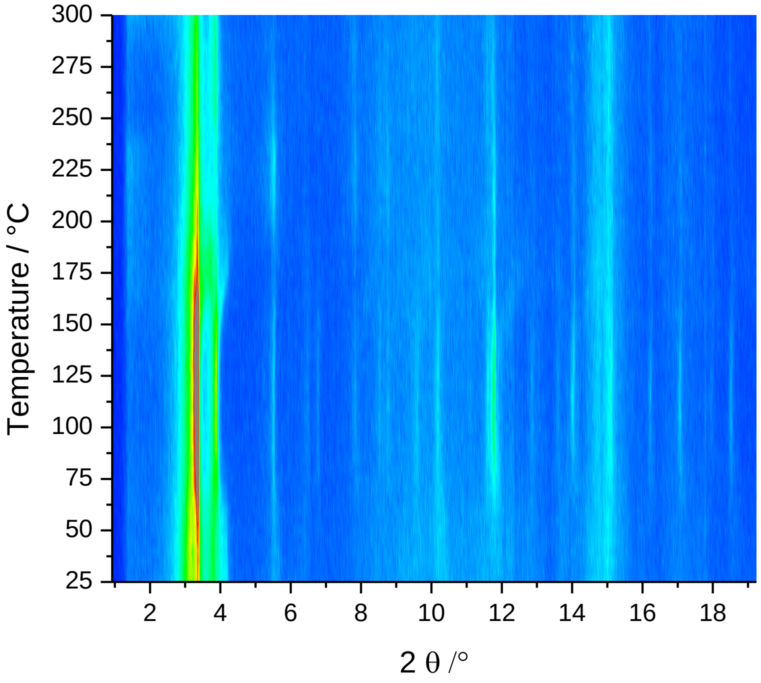

Fig. S9.1. Results of the temperature dependent PXRD investigation of Zr-UiO-66-PDC. The compound is thermally stable up to approximately 220°C.

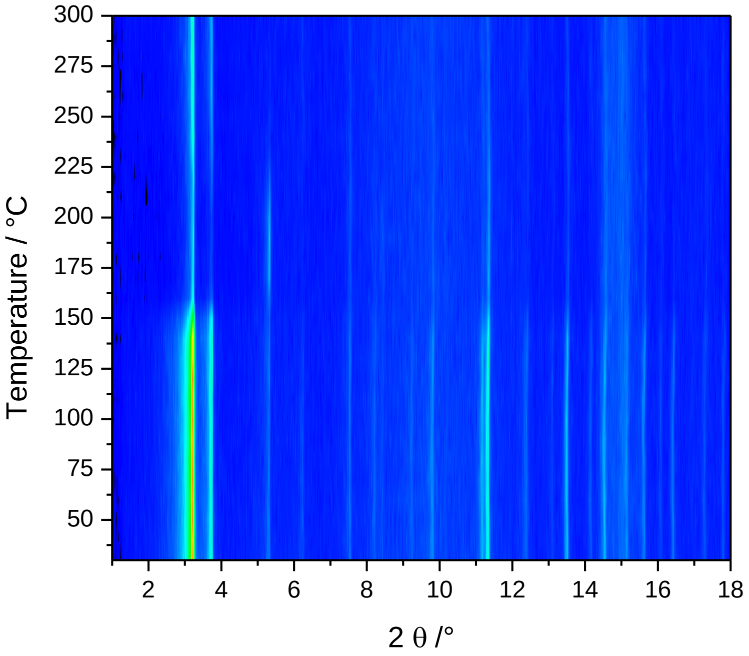

Fig. S9.2. Results of the temperature dependent PXRD investigation of Ce-UiO-66-PDC. The compound is thermally stable up to approximately 150°C.

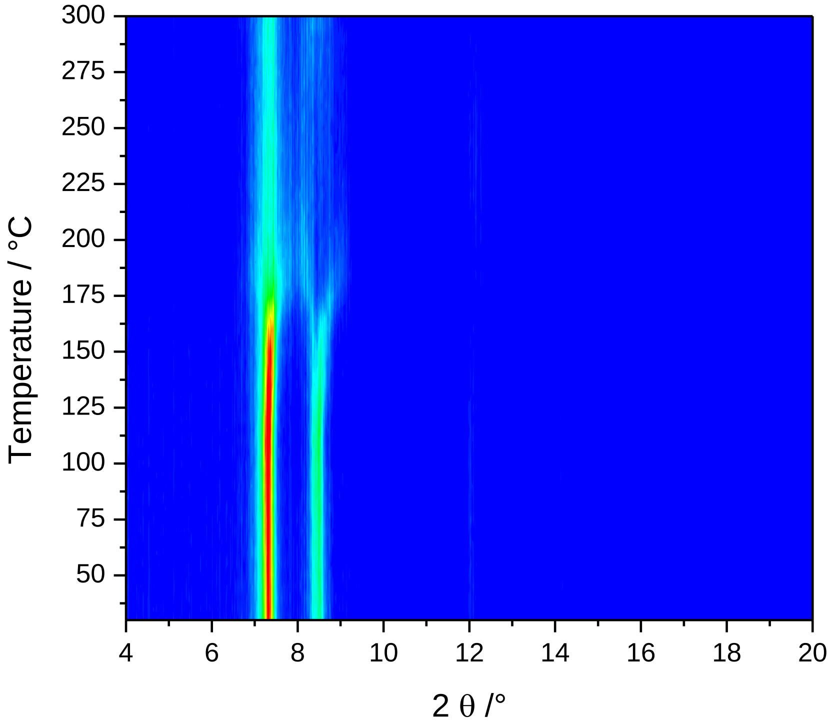

Fig. S9.3. Results of the temperature dependent PXRD investigation of Hf-UiO-66-PDC. The compound is thermally stable up to approximately 150°C.

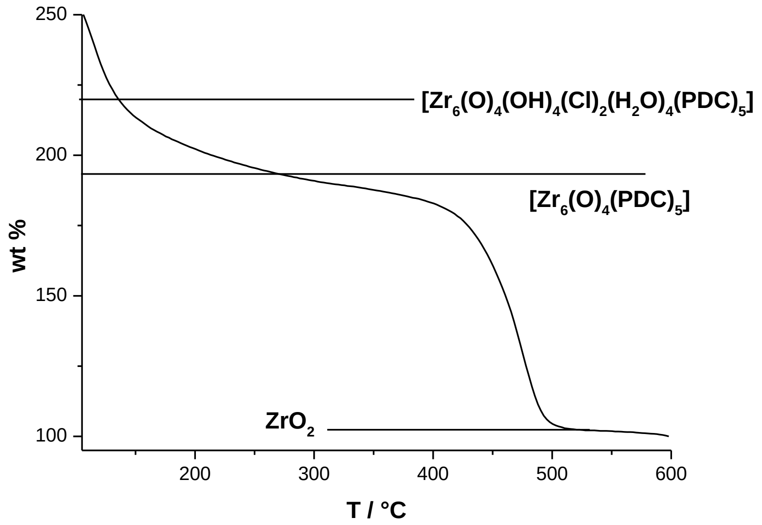

Fig. S9.4. TGA plot for Zr-UiO-66-PDC. The MOF shows a relatively high first weight loss event occurring up on dehydration. Zr-UiO-66-PDC is stable up to 350 °C.

Table S9.1. Comparison of the thermogravimetric analysis of Zr-UiO-66-PDC and the associated mass loss.

Sum formula of postulated product Zr-UiO-66-PDC	**T / °C**	**Theoretical wt %**	**Measured wt %**
$[Zr_6(O)_4(OH)_4(Cl)_2(H_2O)_4(PDC)_5]$	135	220	220
$[Zr_6(O)_4(PDC)_5]$	260	194	194
$6 \cdot ZrO_2$	520	100	100

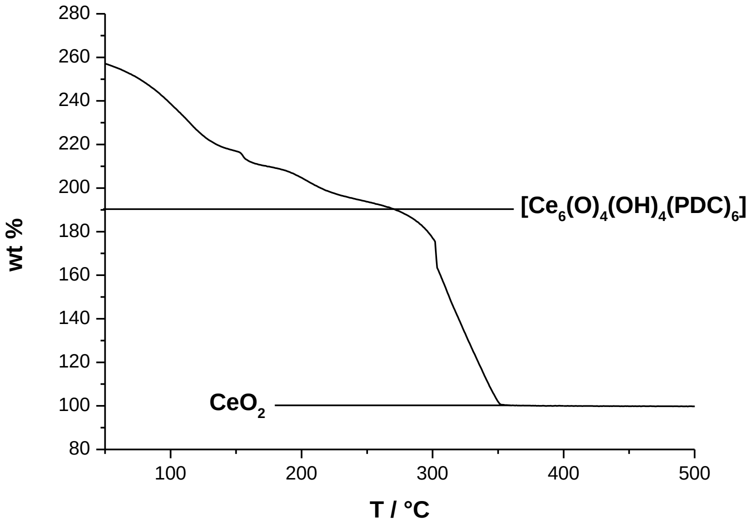

Fig. S9.5. TGA plot for Ce-UiO-66-PDC. The MOF shows a relatively high first weight loss event occurring up on dehydration. Ce-UiO-66-PDC is stable up to 210 °C.

Table S9.2. Comparison of the thermogravimetric analysis of Ce-UiO-66-PDC and the associated mass loss.

Sum formula of postulated product Ce-UiO-66-PDC	T / °C	Theoretical wt %	Measured wt %
$[Ce_6(O)_4(OH)_4(PDC)_6]$	200	190	190
$6{\cdot}CeO_2$	360	100	100

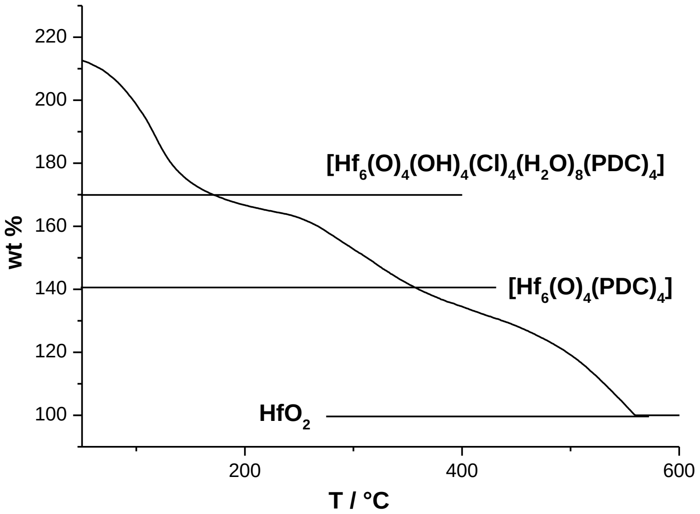

Fig. S9.6. TGA plot for Hf-UiO-66-PDC. The MOF shows a relatively high first weight loss event occurring up on dehydration. Hf-UiO-66-PDC is stable up to 220 °C.

Table S9.3. Comparison of the thermogravimetric analysis of Hf-UiO-66-PDC and the associated mass loss.

Sum formula of postulated product Hf-UiO-66-PDC	T / °C	Theoretical wt %	Measured wt %
$[Hf_6(O)_4(OH)_4\ (Cl)_4(H_2O)_8(PDC)_4]$	170	170	170
$[Hf_6(O)_4(PDC)_4]$	350	141	141
$6{\cdot}HfO_2$	560	100	100

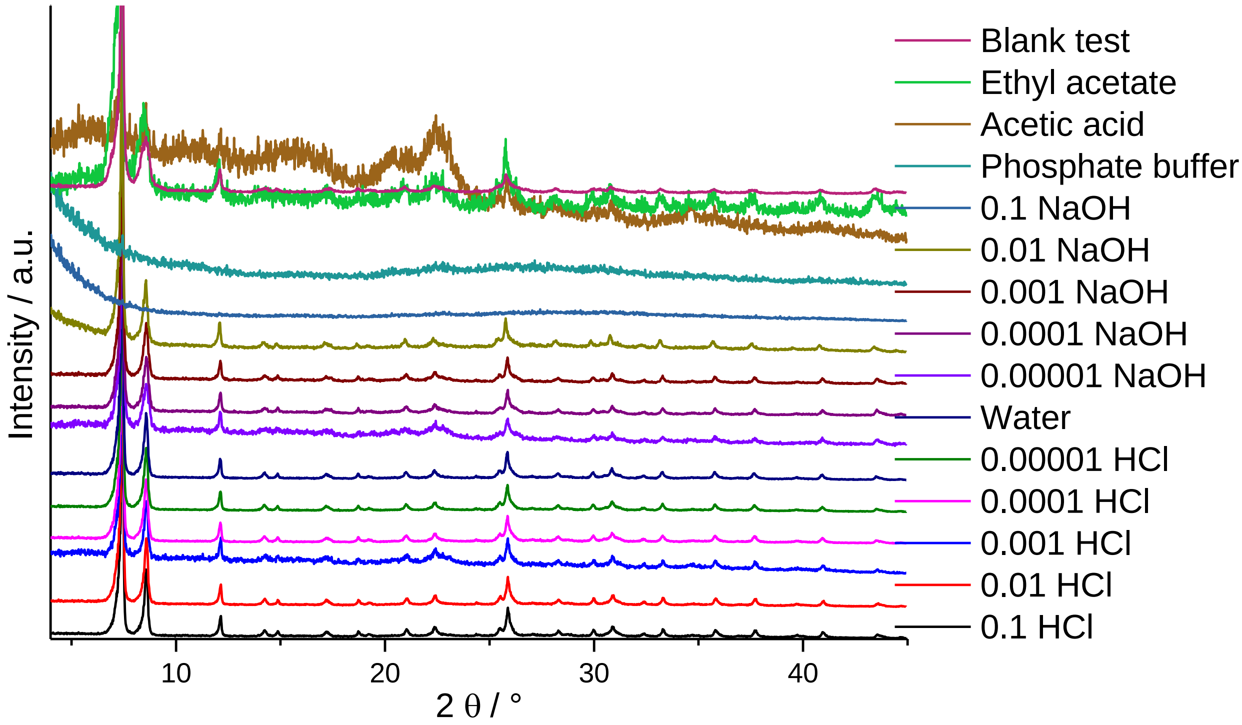

Fig. S9.7. PXRD patterns of Zr-UiO-66-PDC after stirring 25 mg in 1ml of aqueous solutions with different pH-values (different concentrations of HCl and NaOH) for 24 h.

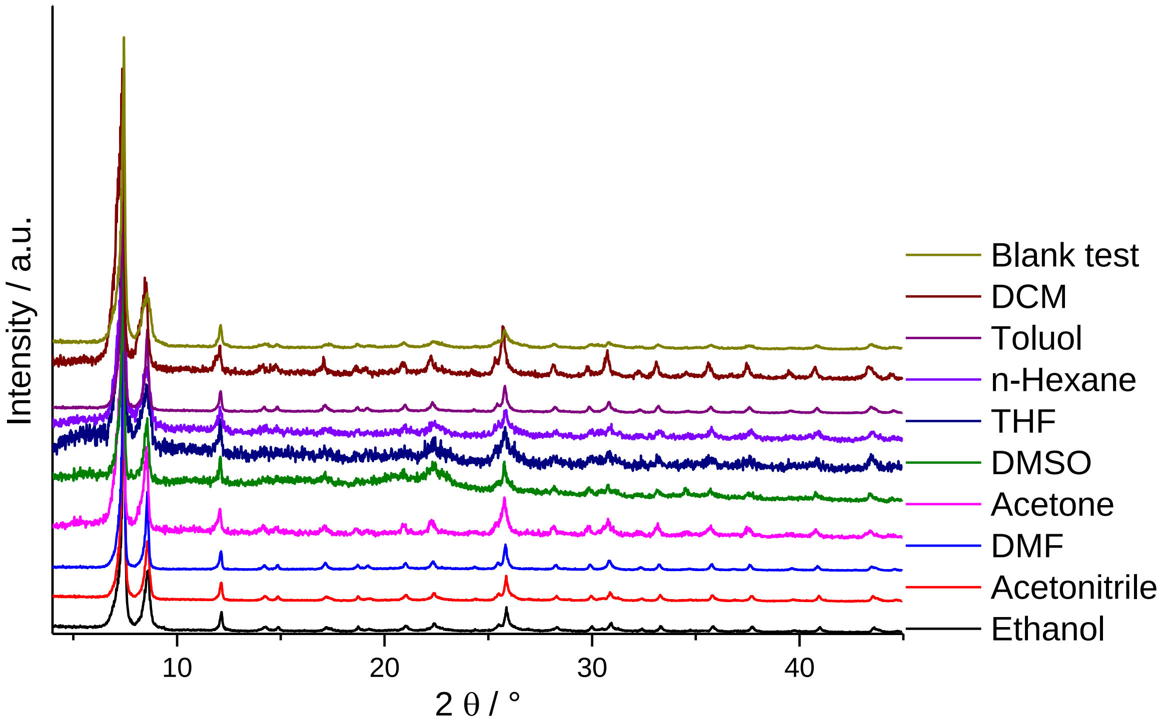

Fig. S9.8. PXRD patterns of Zr-UiO-66-PDC after stirring in different organic solvents for 24 h.

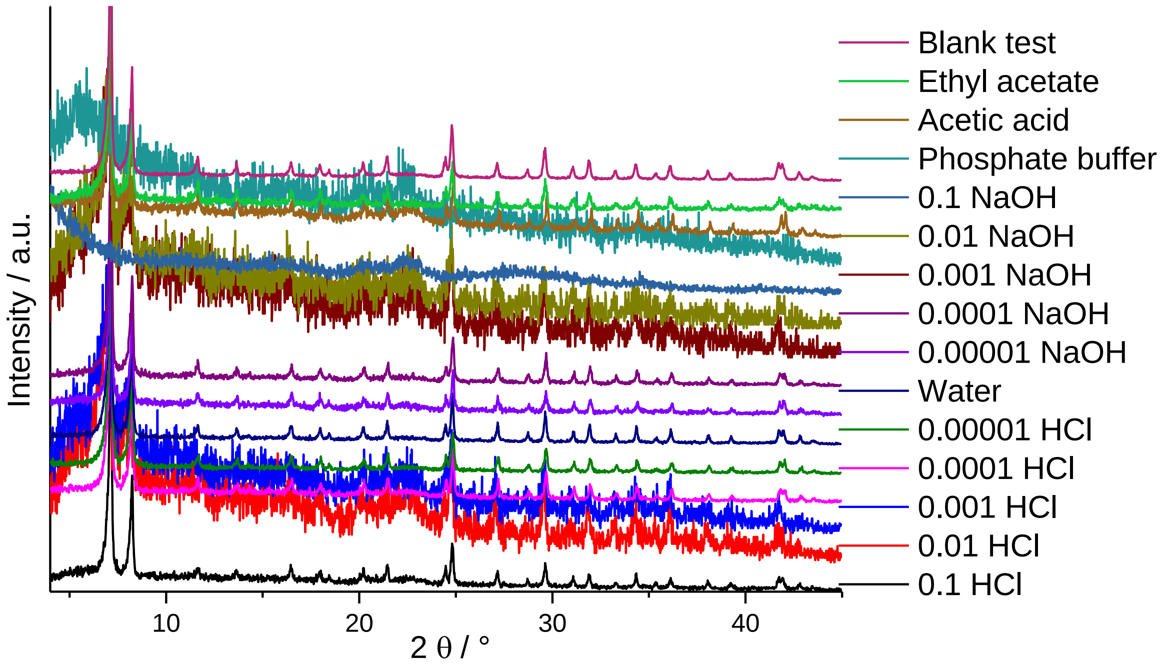

Fig. S9.9. PXRD patterns of Ce-UiO-66-PDC after stirring in aqueous solutions with different pH-values due to different concentrations of HCl and NaOH for 24 h.

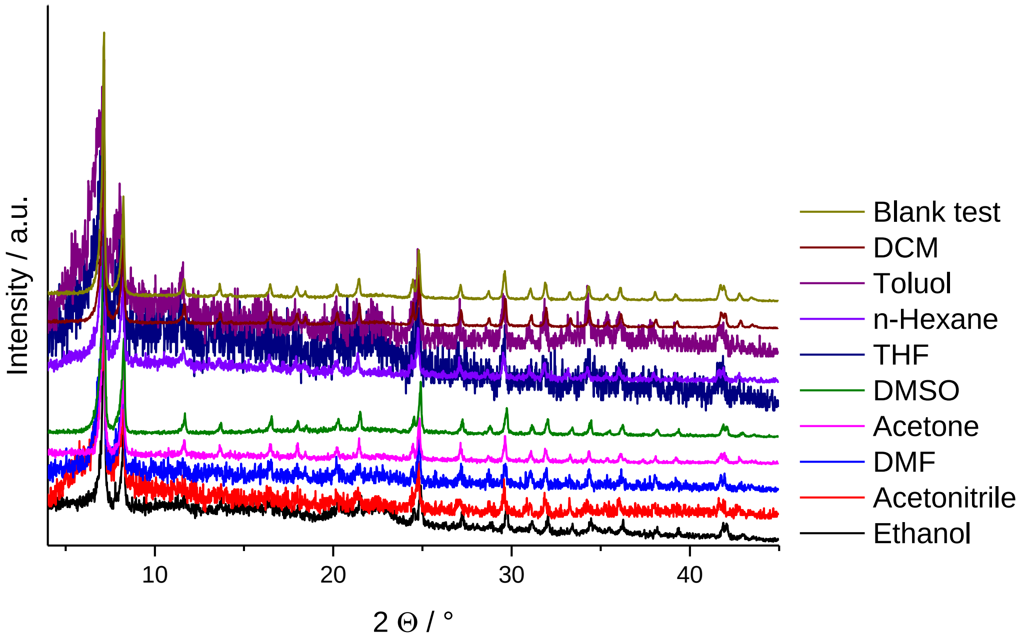

Fig. S9.10. PXRD patterns of Ce-UiO-66-PDC after stirring in different organic solvents for 24 h.

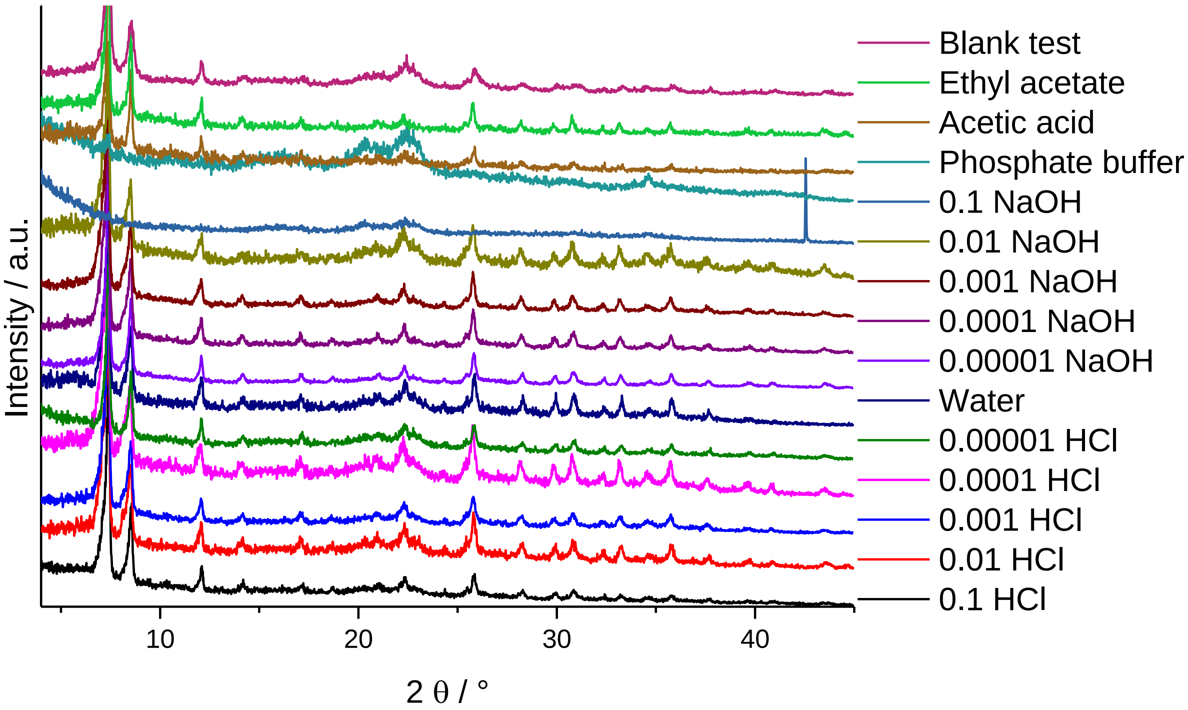

Fig. S9.11. PXRD patterns of Hf-UiO-66-PDC after stirring in aqueous solutions with different pH- values due to different concentrations of HCl and NaOH for 24 h.

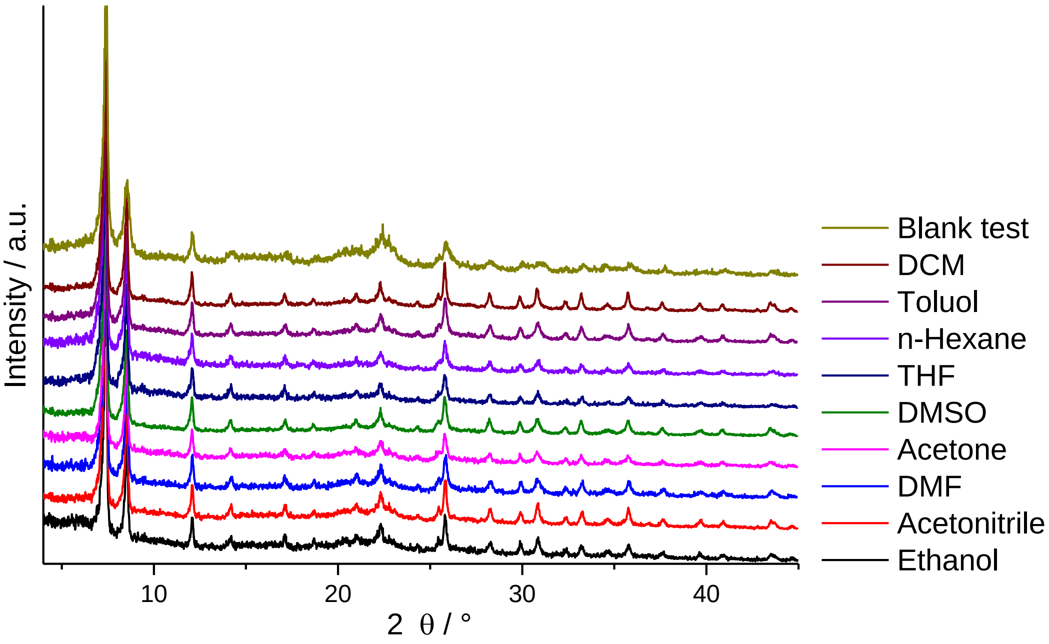

Fig. S9.12. PXRD patterns of Hf-UiO-66-PDC after stirring in different organic solvents for 24 h.

S10 Luminescence Measurements

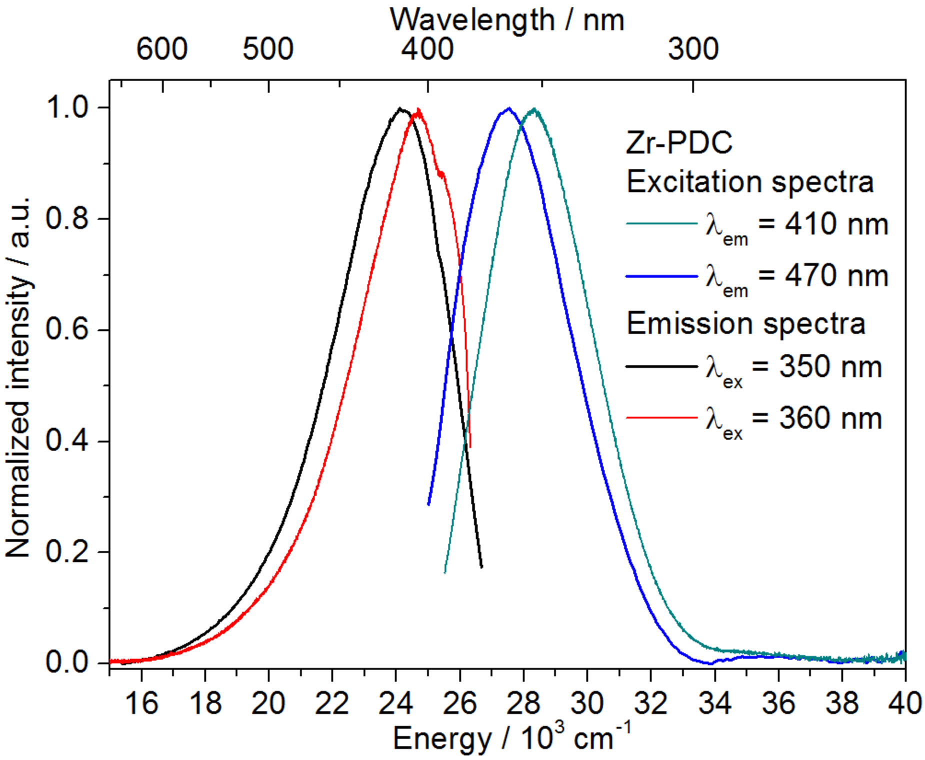

Fig. S10.1. Emission and excitation spectra of Zr-UiO-66-PDC.

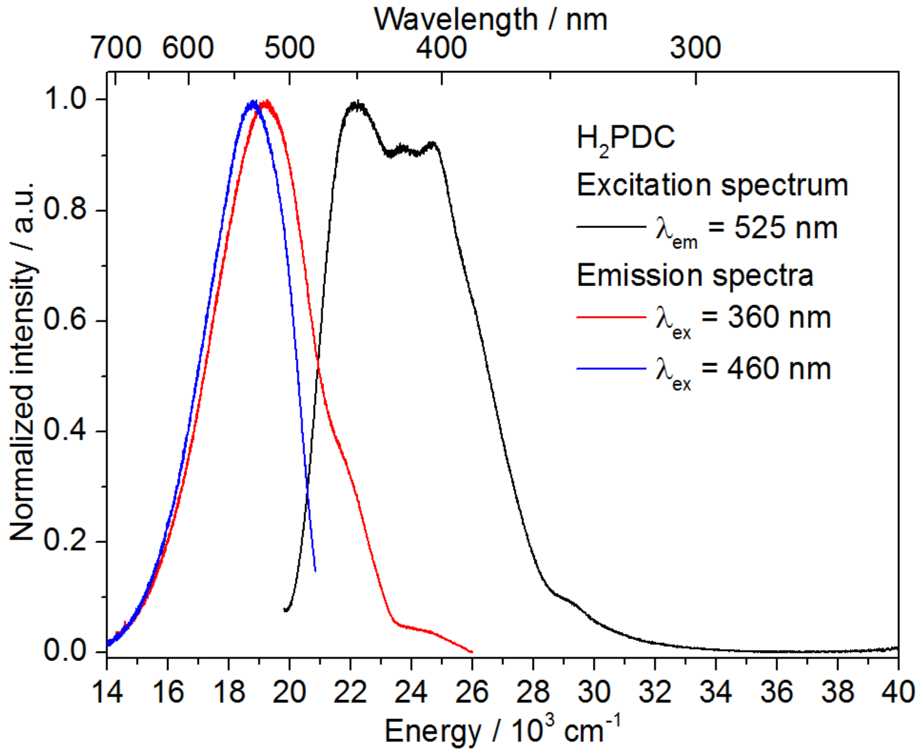

Fig. S10.2. Emission and excitation spectra of H_2PDC.

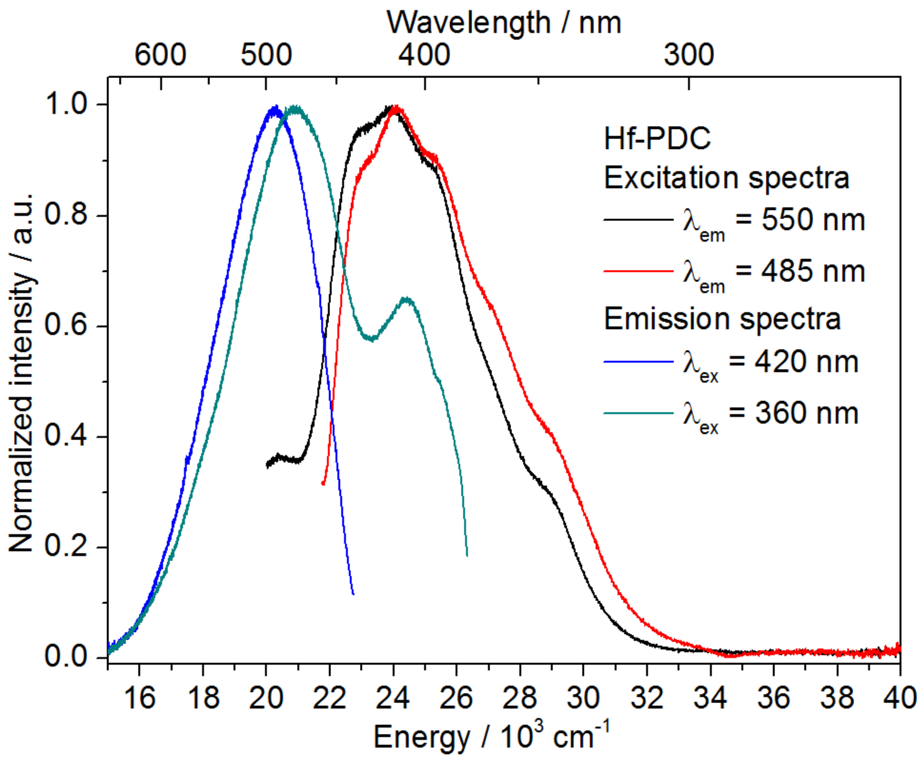

Fig. S10.3. Emission and excitation spectra of Hf-UiO-66-PDC.

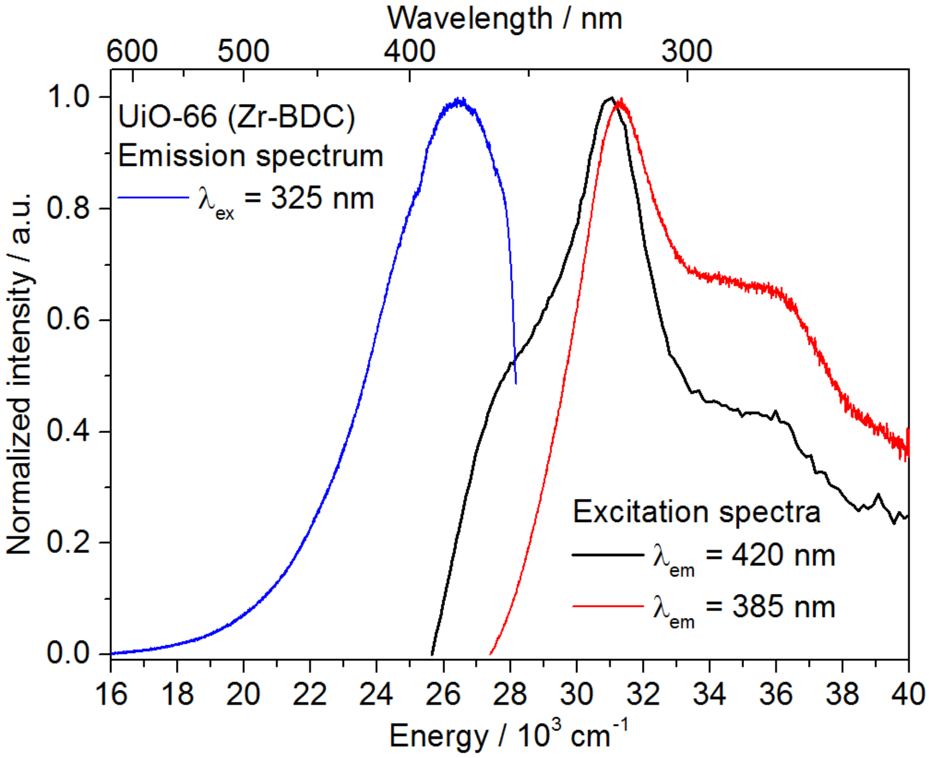

Fig. S10.4. Emission and excitation spectra of Zr-UiO-66-BDC.

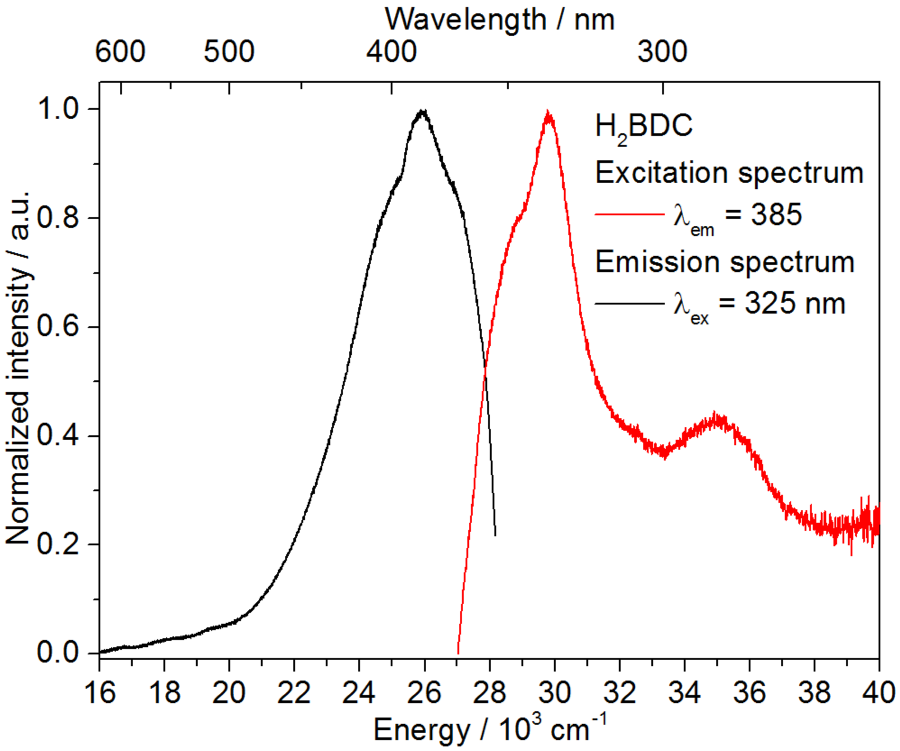

Fig. S10.5. Emission and excitation spectra of H_2BDC.

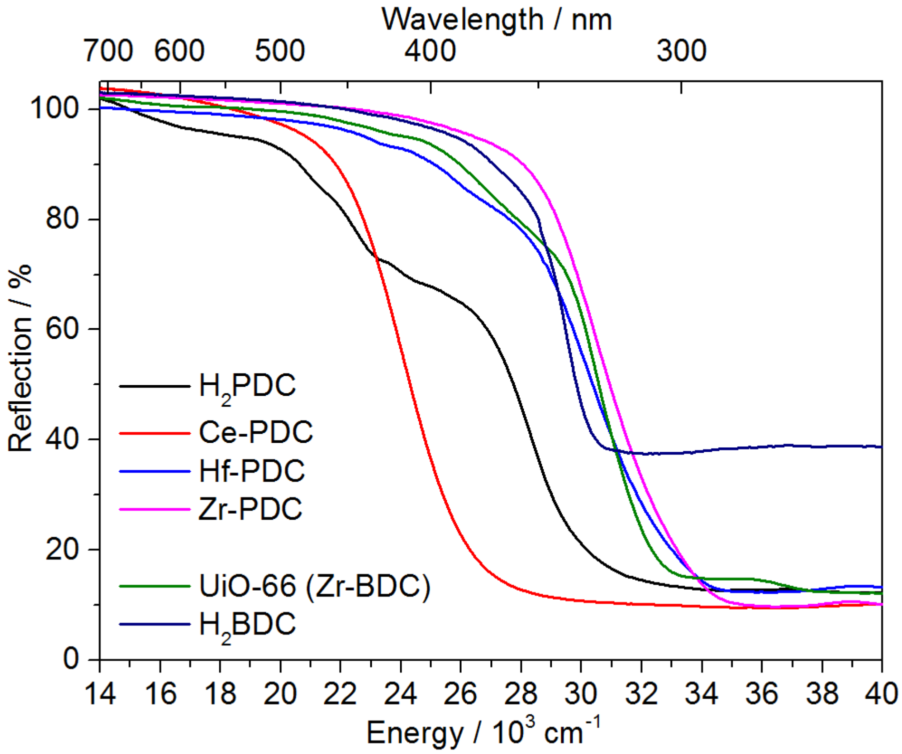

Fig. S10.6. Reflection spectra of H_2PDC, Ce-UiO-66-PDC, Hf-UiO-66-PDC, Zr-UiO-66-PDC, Zr-UiO-66-BDC and H_2BDC, diluted with $BaSO_4$.

S11 M-UiO-66-PDC (M = Zr, Ce, Hf): Sorption Experiments

M-UiO-66-PDC (M = Zr, Ce, Hf) was activated for sorption measurements by heating the sample at 120 °C under dynamic vacuum overnight. All three compounds are porous towards N_2 and CO_2 at -196 °C and 25 °C respectively (Fig. S11.1. and Fig. S.11.3., Tab. S11.1.). The PXRD patterns before and after the activation procedure show no changes with the exclusion of Hf-UiO-66-PDC, which is not stable at this activation condition (Fig. S11.2.).

Tab. S11.1.: The specific surface area ($a_{s,BET}$)and the micropore volume ($V_{mic.}$) (left) based on nitrogen adsorption and the total CO_2 uptake with the corresponding pressure (right) of M-UiO-66-PDC with M = Zr, Ce, Hf and the corresponding UiO-66-BDC compounds.

MOF	$a_{s,BET}$ / m^2 g^{-1}	$a_{s,BET}$ / m^2 $mmol^{-1}$	$V_{mic.}$ / cm^3 g^{-1}	Capacity / mg g^{-1}	Capacity / mg $mmol^{-1}$	p / bar
Zr-UiO-66-PDC	1376	2267	0.54	200	330	1
Zr-UiO-66-BDC[7],[8]	1105	---	---	240	---	18
Ce-UiO-66-PDC	768	1505	0.24	100	196	1
Ce-UiO-66-BDC[9]	1282	---	0.50	---	---	---
Hf-UiO-66-PDC	383	823	0.18	---	---	---
Hf-UiO-66-BDC[10]	358 - 749	---	0.15 – 0.35	---	---	---

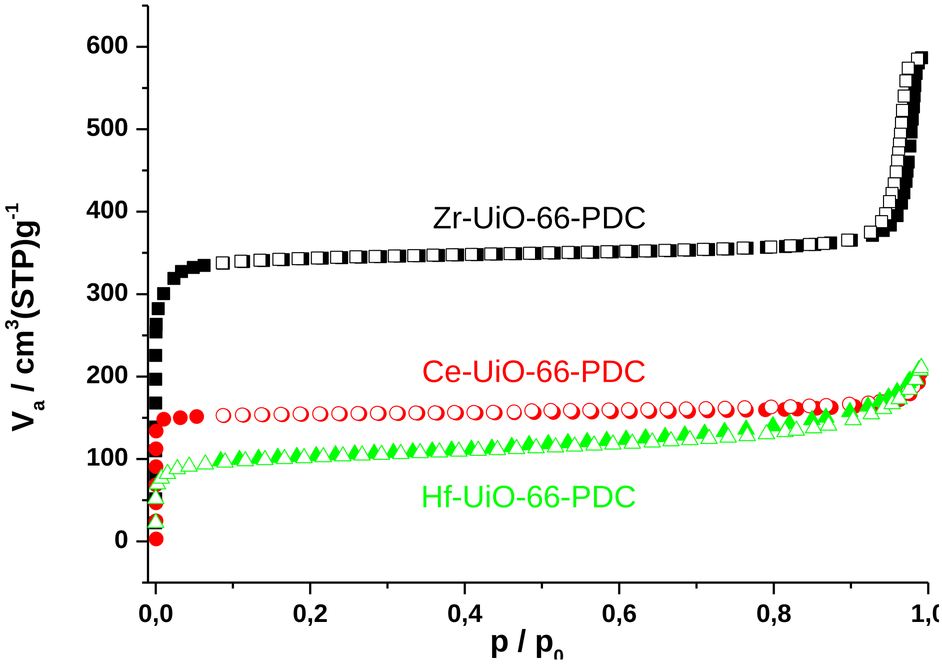

Fig. S11.1. N_2-adsorption and desorption isotherms for M-UiO-66-PDC with M = Zr, Ce, Hf measured at -196 °C.

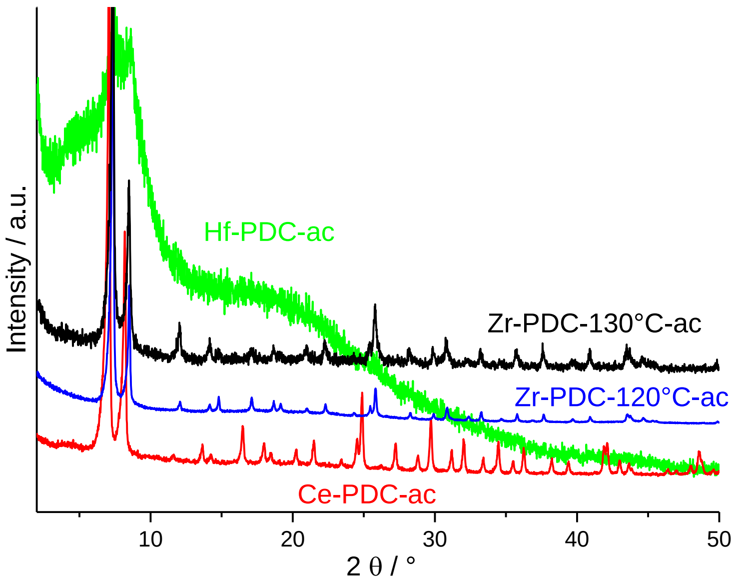

Fig. S11.2. PXRD patterns (λ = Cu K$_{\alpha 1}$) of M-UiO-66-PDC with M = Zr, Ce, Hf after activation and after N_2 sorption experiment.

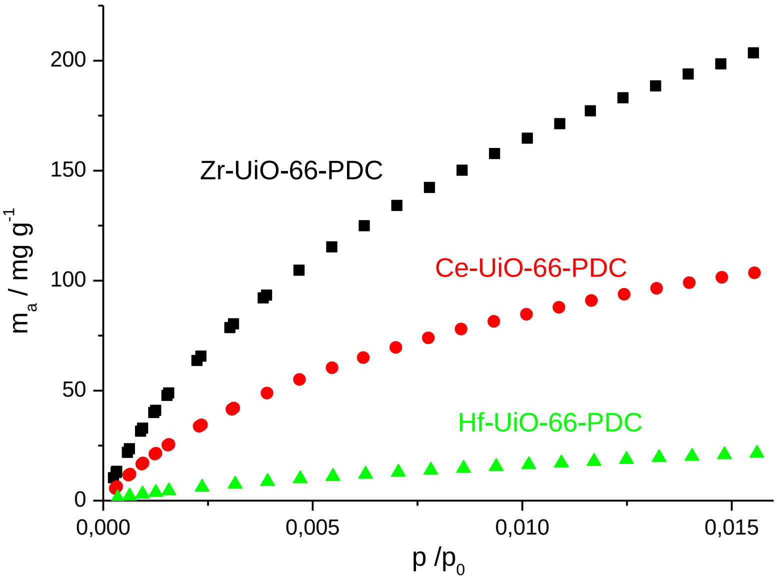

Fig. S11.3. CO_2-adsorption isotherms of M-UiO-66-PDC with M = Zr, Ce, Hf measured at 25 °C.

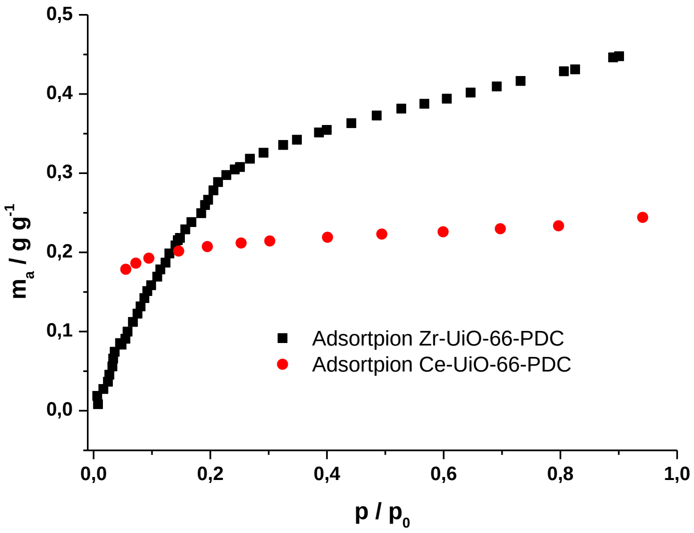

Fig. S11.4. H_2O-adsorption isotherms of M-UiO-66-PDC with M = Zr and Ce measured at 25 °C.

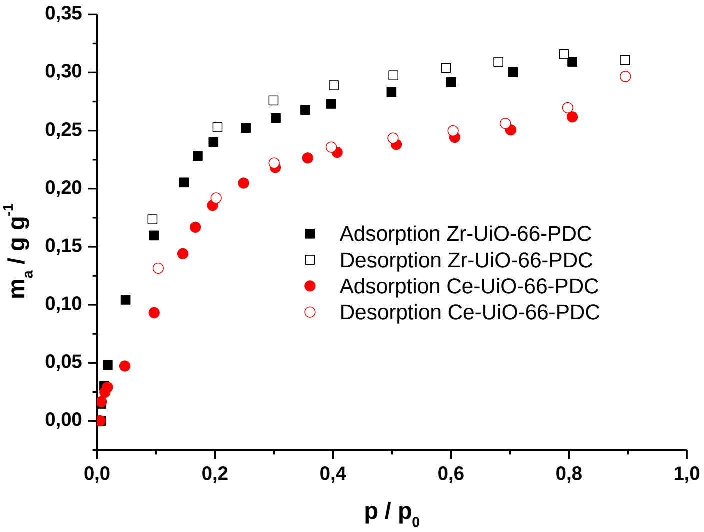

Fig. S11.5. MeOH-adsorption and desorption isotherms of M-UiO-66-PDC with M = Zr and Ce measured at 25 °C.

Tab. S11.2.: The H_2O (left) and MeOH (right) uptake with the corresponding pressure of M-UiO-66-PDC with M = Zr and Ce and the corresponding UiO-66-BDC compounds.

MOF	H_2O			MeOH		
	Capacity / g g^{-1}	Capacity / g $mmol^{-1}$	α	Capacity / g g^{-1}	Capacity / g $mmol^{-1}$	α
Zr-UiO-66-PDC	0.34	0.56	0.01 - 0.2	0.31	0.51	0.2
Zr-UiO-66-BDC[11]	0.40	---	0.4	---	---	---
Zr-UiO-66-BDC-NH_2[11]	0.34	---	0.25	---	---	---
Ce-UiO-66-PDC	0.23	0.45	0.1	0.30	0.59	0.2

S12 Cycling water vapor sorption experiments

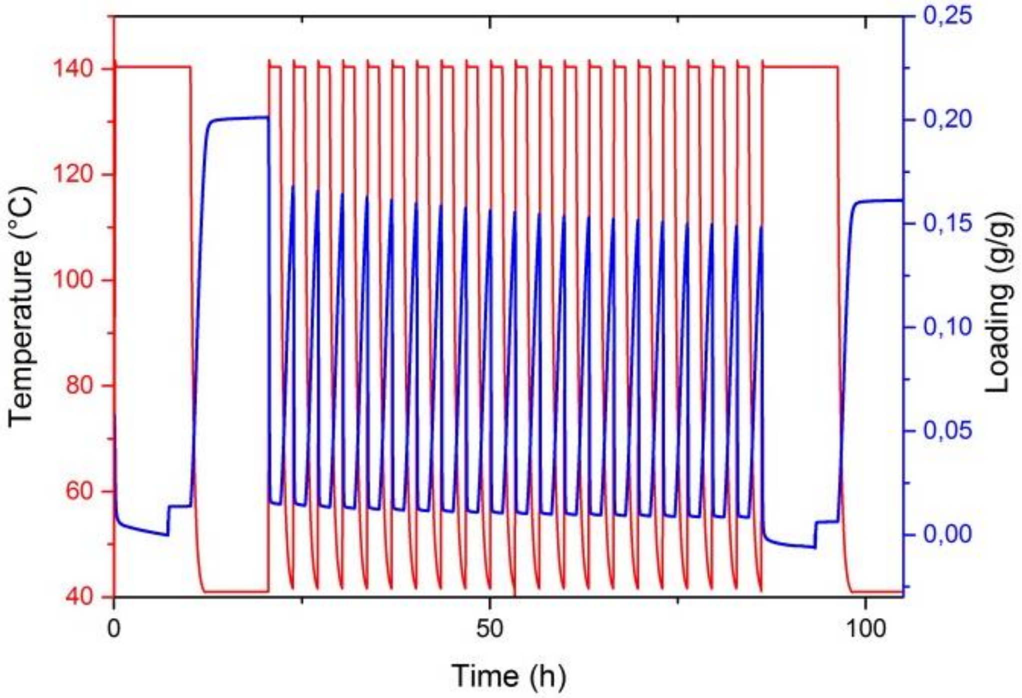

Fig. S12.1: Thermogravimetric adsorption/desorption cycling experiments for 20 cycles of Ce-UiO-66-PDC. Long segments at the beginning and at the end of each experiment were conducted to determine the equilibrium loading of the sample. Ce-UiO-66-PDC shows nearly no loss of dry mass, the degradation is visible in loss of uptake capacity, from 0.20 g/g to 0.16 g/g (20 %). This larger degradation could also be due to the applied desorption temperature of 140 °C and the low thermal stability of Ce-UiO-66-PDC.

S13 In situ DRIFTS measurements

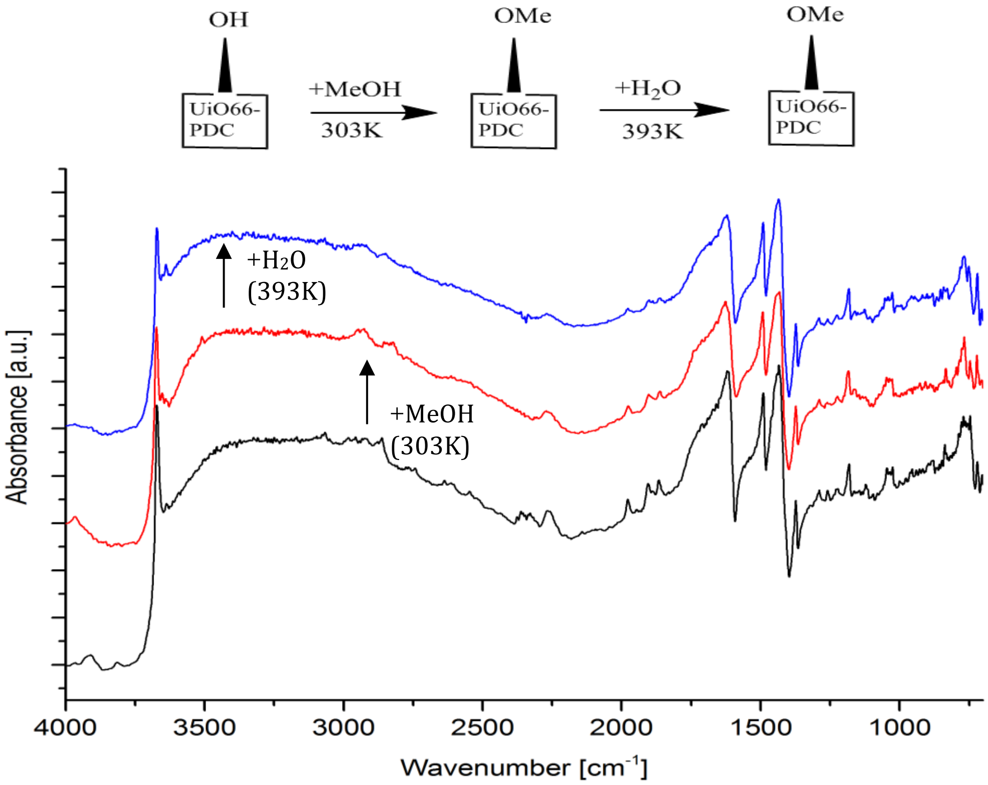

Fig.S13.1: Comparison of UiO-66-PDC treatments. Black: UiO-66-PDC; Red: Treatment with methanol wetted gas stream at 303K for 15 minutes; Blue: Treatment with humidified nitrogen stream at 393K for 30 min to investigate if back exchange of methoxy groups to hydroxyl groups occurs. All spectra were recorded under dry N_2 (after reaching equilibrium) at 303K and are shown with a shift in the y-axis for better comparison. No back exchange from the methoxy group through the hydroxyl group could be observed.

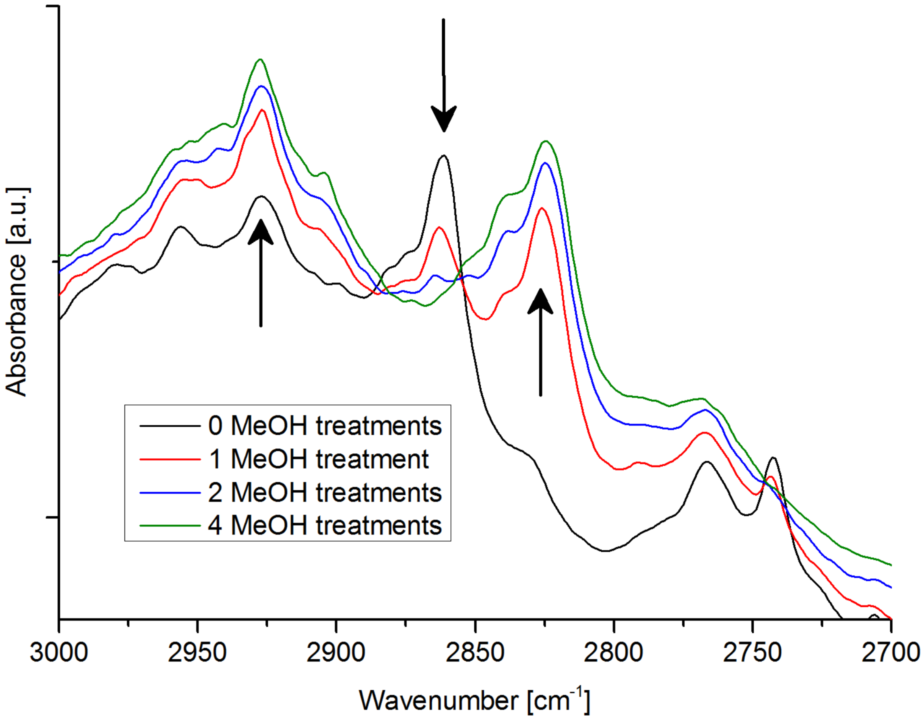

Fig. S13.2: In situ DRIFTS measurements. Measurement at 393 K under N_2 gas atmosphere with a flow rate of 100 ml/min. The sample of Zr-UiO-66-PDC was subjected 5 times to a nitrogen stream mixed with MeOH for 30 seconds. For this, the N_2 stream was passed through a MeOH bath (298 K) with a bubble diffusor. After each treatment the sample was treated with dry N2 until equilibrium and the spectrum was recorded. Arrows indicate the bands that are due to vibrations of the -CH_3 group of methanol (increase at 2927 and 2824 cm^{-1}) and the bridging OH group (decrease at 2861 cm^{-1}).[12]

S14 References

1. A. Topas Academics 4.2; Coelho Software: Brisbane, **2007**.
2. B. Ravel and M. Newville, ATHENA, ARTEMIS, HEPHAESTUS: data analysis for X-ray absorption spectroscopy using IFEFFIT, *J. Synchrotron Rad.*, 2005, **12**.
3. J.J. Rehr and R.C. Albers, *Rev. Mod. Phys.*, 2000, **72**.
4. G.C. Shearer, S. Chavan, J. Ethiraj, J.G. Vitillo, S. Svelle, U. Olsbye, C. Lamberti, S. Bordiga, and K.P. Lillerud, *Chem. Mater.*, 2014, **26**.
5. L. Valenzano, B. Civalleri, S. Chavan, S. Bordiga, M.H. Nilsen, S. Jakobsen, K.P. Lillerud, and C. Lamberti, *Chem. Mater.*, 2011, **23**.
6. S. Øien, D. Wragg, H. Reinsch, S. Svelle, S. Bordiga, C. Lamberti, and K.P. Lillerud, *Cryst. Growth Des.*, 2014, **14**.
7. G. C. Shearer, S. Chavan, J. Ethiraj, J. G. Vitillo, S. Svelle, U. Olsbye, C. Lamberti, S. Bordiga and K. P. Lillerud, *Chem. Mater.*, 2014, **26**.
8. K. Sumida, D. L. Rogow, J. A. Mason, T. M. McDonald, E. D. Bloch, Z. R. Herm, T.-H. Bae, J. R. Long, *Chem. Rev.,* 2012, **112**.
9. M. Lammert, M. T. Wharmby, S. Smolders, B. Bueken, A. Lieb, K. A. Lomachenko, D. D. Vos and N. Stock, *Chem Commun*, 2015, **51**.
10. M. J. Cliffe, W. Wan, X. Zou, P. A. Chater, A. K. Kleppe, M. G. Tucker, H. Wilhelm, N. P. Funnell, F.-X. Coudert and A. L. Goodwin, *Nat. Commun.*, 2014, **5**.
11. F. Jeremias, V. Lozan, S. K. Henninger, C. Janiak, *Dalton Trans.,* 2013, **45**.
12. D. Yang, V. Bernales, T. Islamoglu, O. K. Farha, J. T. Hupp, C. J. Cramer, L. Gagliardi and B. C. Gates, *J. Am. Chem. Soc.*, 2016, **138**.